Published in final edited form as:

Structure. 2023 May 04; 31(5): 553–564.e7. doi:10.1016/j.str.2023.02.011.

Structures of Ric-8B in complex with Gα protein folding clients reveal isoform specificity mechanisms

Makaía M. Papasergi-Scott[1,4], **Frank E. Kwarcinski**[2,4], **Maiya Yu**[2,4], **Ouliana Panova**[1], **Ann M. Ovrutsky**[2], **Georgios Skiniotis**[1,3,*], **Gregory G. Tall**[2,5,*]

[1]Department of Molecular and Cellular Physiology, Stanford University School of Medicine, Stanford, CA 94305, USA

[2]Department of Pharmacology, University of Michigan School of Medicine, Ann Arbor, MI 48109, USA

[3]Department of Structural Biology, Stanford University School of Medicine, Stanford, CA 94305, USA

[4]These authors have contributed equally.

[5]Lead contact.

Summary

Mammalian Ric-8 proteins act as chaperones to regulate the cellular abundance of heterotrimeric G protein α subunits. The Ric-8A isoform chaperones Gαi/o, Gα12/13, and Gαq/11 subunits, while Ric-8B acts on Gαs/olf subunits. Here, we determined cryoEM structures of Ric-8B in complex with Gαs and Gαolf, revealing isoform differences in the relative positioning and contacts between the C-terminal α5 helix of Gα within the concave pocket formed by Ric-8 α-helical repeat elements. Despite the overall architectural similarity with our earlier structures of Ric-8A complexed to Gαq and Gαi1, Ric-8B distinctly accommodates an extended loop found only in Gαs/olf proteins. The structures, along with results from Ric-8 protein thermal stability assays and cell-based Gαolf folding assays, support a requirement for the Gα C-terminal region for binding specificity, and highlight that multiple structural elements impart specificity for Ric-8/G protein binding.

*Correspondence: yiorgo@stanford.edu (G.S.); gregtall@med.umich.edu (G.G.T.).

Author Contributions

M.M.P.-S. prepared EM grids; collected, processed, analyzed, modeled, and rendered cryoEM data; and analyzed results. F.E.K. prepared DNA constructs, purified proteins, conducted cell-based mutagenesis studies, and performed thermo-stability assays. M.Y. prepared DNA constructs, purified proteins and performed thermo-stability assays. O.P. prepared EM grids and collected cryoEM data. A.M.O. performed Western Blot characterization of protein levels. G.G.T. prepared DNA constructs and purified proteins. G.S. and G.G.T. supervised the project. M.M.P.-S., F.E.K., M.Y., G.S, and G.G.T wrote the manuscript.

Declaration of Interests

G.S. is a co-founder of and consultant for Deep Apple Therapeutics.

Movie S1. 3D variability analysis (simply display) of the first principal component (PC0), Related to Figures 5 and S7. Ric-8B colored in teal, and Gαs colored in gold. *Multimedia file,* mp4 format.

Table S5. Raw data, Related to Figures 4, S1, S3, S4, Table S1, and STAR Methods. *Excel spreadsheet.*

GRAPHICAL ABSTRACT

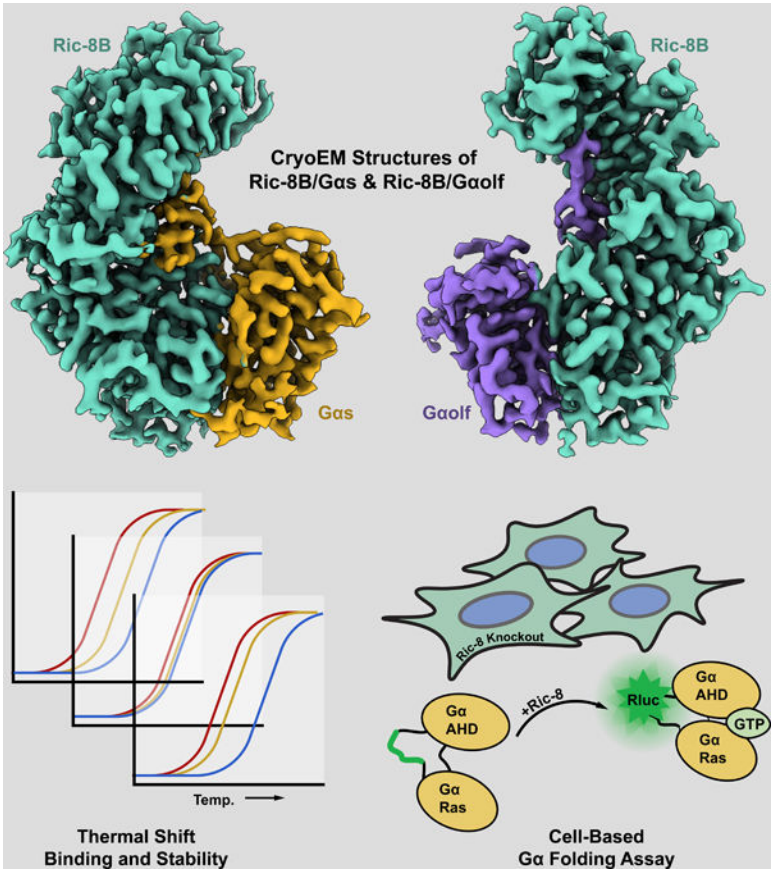

eTOC:

Papasergi-Scott et al. present the cryo-EM structures of Ric-8B in complex with open, nucleotide-free Gαolf and Gαs. These structures provide molecular insight into the process of Gα subunit protein folding and define a basis for Ric-8A and Ric-8B specificity differences for Gα subunit substrates.

Keywords

G protein alpha subunit; Resistance to Inhibitors of Cholinesterase-8; Ric-8; chaperone; cryoEM; structure; GEF; Gαs; olfactory; Gαolf

Introduction

G protein-coupled receptors (GPCRs), the largest class of eukaryotic membrane proteins, play central physiological roles in intracellular communication through a remarkable diversity in ligand recognition, tissue-specific expression, and transducer activation. Vital to GPCR mediated responses is the activation of heterotrimeric G proteins, which consist of a Gα subunit and an obligate Gβγ heterodimer. G protein coupling to activated GPCRs promotes rearrangement of the Gα C-terminus and α5 helix, leading to global

changes in G protein conformation that facilitate the release of GDP and subsequent binding of GTP by the Gα subunit. GTP binding reorders the Gα switch regions (SwI-SwIII) to enable functional dissociation from the Gβγ heterodimer and activation of downstream effectors.[1–3] Different GPCRs can selectively or promiscuously activate G protein heterotrimers composed of 15 human Gα subunits that are divided into four classes, Gαs, Gαi/o, Gαq/11, and Gα12/13, based on sequence similarity and the distinct downstream effectors that each class engages.

The integral role of G protein signaling is underpinned by strict biosynthetic quality control mechanisms. The production and circulation of heterotrimeric G proteins is enabled by multiple chaperones, including the chaperonin-containing tailless complex polypeptide-1 (CCT-1) that mediates Gβ folding[4], the dopamine receptor-interacting protein 78 (DRiP78) that may assist Gγ folding[5], and the phosducin-like protein 1 (PhLP1) that facilitates the formation of Gβγ heterodimers[6–8]. Ric-8 proteins act as Gα subunit guanine nucleotide exchange factors (GEFs) *in vitro*, which led to their initial assignment as G protein signaling regulators[9–11]. However, subsequent work using *Ric-8* gene deletion models, found that Gα protein abundances were reduced[10,12–21], an observation later delineated to be an effect of Gα subunit misfolding leading to increased G protein turnover.[12,22] Taken together, the findings have been consistent with Ric-8 proteins acting as *bona fide* molecular chaperones that enable properly folded Gα subunits[23].

Lower-order species, such as flies, worms, and slime-molds, possess only a single isoform of Ric-8 that is presumed to act on all respective ancestral Gα classes.[24] In mammals, the folding of all 15 Gα subunits is assisted by Ric-8A and Ric-8B.[12,22] Ric-8A facilitates the biosynthesis of Gα subunits of the Gi/o, Gq/11, and G12/13 classes, while Ric-8B is specific for the Gs class of Gα subunits. Notably, Ric-8 interactions with Gα subunits are highly specific, as Ric-8A does not bind Gαs class proteins with appreciable activity,[11] nor does Ric-8B engage Gαi class proteins. However, Ric-8B can bind Gαq and Gα12/13 at high protein concentrations *in vitro*.[9] The structural basis of Ric-8 and Gα subunit client protein specificity remain an open question.

Though the Gαs class encompasses only two of the fifteen Gα types, it contains the essential olfactory/brain-specific Gαolf subunit. Given that the majority of GPCRs are olfactory receptors, understanding Golf action is vital, yet its characterization has proven elusive due to challenges in purifying Gαolf in sufficient quantity. While recombinant Gαs is readily purified from *E. coli*, which is devoid of endogenous Ric-8, Gαolf abundance is highly dependent on Ric-8B for poorly understood reasons.[25–27] Indeed, primary characterization of purified Gαolf was only permitted through development of a method that involved Ric-8 association for purifying G protein α subunits.[28] Additionally, co-transfection of Ric-8B with Gαolf allowed functional reconstitution of odorant receptor signaling in heterologous cells.[25,26] Moreover, mice with conditional *Ric-8b* deletion in olfactory neurons are anosmiac, a genetic effect attributed to Gαolf dysfunction.[29]

X-ray crystallography studies of truncated Ric-8A spanning residues 1–452 or 1–492 (of 530 residues) (PDB ID: 6NMD[30]; PDB ID: 6N86[31]) showed that the core of the protein consisted of armadillo (ARM) and Huntington, Elongation Factor 3, PR65/A, TOR1 (HEAT)

α-helical repeat elements. A complex of Ric-8A 1–492 bound to a fusion of maltose-binding protein with a 14-mer C-terminal peptide of Gα-transducin (GαT), a member of the Gαi-class of G proteins (PDB ID: 6N85[31]), showed that the GαT peptide became helically ordered when bound within a concave cavity formed by the Ric-8A ARM/HEAT repeats. The phosphorylation of two conserved Ric-8A phosphorylated residues, S435 and T440, was found to be required for Ric-8A chaperone and GEF activities, and also enabled stable complexation between Ric-8 and Gα. More recent cryoEM structures, including our own, of full-length Ric-8A in complex with Gαq (PDB ID: 6VU5) and $G\alpha i_1$ (PDB IDs: 6VU8, 6TYL, 6UKT)[30,32,33] revealed multiple interaction sites between Ric-8A and Gα, including the Gα C-terminus/α5 helix, the β-sheet face of the G protein Ras-like domain, and Switch II. Notably, the segment following the Ric-8A helical region (1–420) forms a loop (421–473), positioned by the critical phosphorylated residues, that wraps around the Gα Ras-like domain to form a helical tail (474–483) adjacent to the G protein SwII region.

To gain insights into Ric-8 isoform specificity for different subsets of G proteins, we determined structures of the Ric-8B isoform in complex with its substrates, $G\alpha s_{short}$ and Gαolf. Complementing the structural work, we conducted Ric-8 protein thermal stability assays and developed a novel cell-based Gα protein folding assay to probe features and structural elements of Ric-8 and Gα subunits that are required for productive interaction. The results reinforce the requirement of the Gα α5 helix and the adjacent C-terminal amino acids for binding to Ric-8B. Despite an overall architectural similarity with the earlier structures of Ric-8A in complex with Gαq or $G\alpha i_1$, Ric-8B distinctly accommodates the extended αG-α4 loop (i3) found only in Gαs and Gαolf. However, sequence swapping and deletions did not produce a gain of function in Ric-8A to bind Gαs. Instead, Gαolf deletion and region-specific substitution between the Ric-8 isoforms and homologs highlight that multiple elements impart specificity for Ric-8 / G protein binding, including interactions of Gα Switch II, the α5-helix, and the αG-α4 (i3) loop with the Ric-8 concave surface, extended cradle loop, and helix region.

Results

CryoEM structures of Ric-8B in complex with Gαs and Gαolf

For structural studies of Ric-8B/Gαs and Ric-8B/Gαolf complexes, we expressed and purified recombinant murine Ric-8B (accession: A0A6I9LYN2), human $G\alpha s_s$, and human Gαolf separately from *Trichoplusia ni* insect cells (Figure S1). Since our previous work revealed that phosphorylation of residues Ser435 and Thr440 was crucial for Ric-8A chaperoning and GEF activities,[34] and also enhanced Ric-8A/Gα complex stability for structural studies,[30,32,33] we used protein kinase CK2 to fully phosphorylate the equivalent residues of purified Ric-8B (Ser468 and Thr473).[34,35] Mass spectrometry and immunoblot analyses confirmed Ric-8B phosphorylation at these and additional positions, with phosphorylated Ric-8B having substantially increased thermal stability (ΔTm ~5–6 °C) (Figure S1, Table S1). Because Ric-8 affinity for Gα subunits is maximal in the absence of nucleotide, phosphorylated Ric-8B/Gαs and /Gαolf complexes were assembled and treated with apyrase to eliminate guanine nucleotides.

CryoEM structures of nucleotide-free Ric-8B/Gαs and Ric-8B/Gαolf complexes were determined at global indicated resolutions of 2.8Å and 3.2Å, respectively (Figures 1 and S2, Table S2). The structures of Ric-8B/Gαs and Ric-8B/Gαolf were highly similar with a root-mean-square deviation (RMSD) value of 0.4Å. The overall architecture of Ric-8B is like that of Ric-8A, including a crescent-shaped super-helical structure comprising five ARM and four HEAT repeats, followed by a unique structure that adopts a cradle-like scaffold comprising an extended loop of 12 residues followed by an α-helix (hereby termed the cradle-loop-helix, CLH) (Figure 1E). Reflecting its dynamic nature, the CLH density is only resolved at relatively low resolution, enabling the modeling of its peptide backbone but lacking sufficient detail for confident side-chain modeling (Figure S2). The Ric-8B CLH was followed by a flexible C-terminal region (residues 518–560). Similar to previous structures of Ric-8A/Gαq (PDB ID: 6VU5[33]) and Ric-8A/$G\alpha i_1$ (PDB ID: 6VU8[33], 6TYL[32]), the Gαs/olf Ras-like domain (RLD) and α5 helix were well represented by high resolution features, while the G protein α-helical domain (AHD) was unresolved, presumably due to high flexibility. Our cryoEM maps also confirmed phosphorylation of Ric-8B residues Ser468 and Thr473 (Figures S2K and S2U). As with Ric-8A, phosphorylation of Ric-8B residues Ser468 and Thr473 within a highly conserved acidic cluster of ~12 residues orients the positioning of the CLH through intramolecular contacts with a positively charged patch of residues (Arg378, Arg381, Lys382, Lys385, and Lys441).[34]

An earlier study using limited trypsinization identified proteolytic resistant fragments of Ric-8A consisting of residues 1–428, 1–457, and 1–492 (equivalent Ric-8B residues, 1–462, 1–490, and 1–526, respectively).[36] These protease-resistant regions correlate with the ultra-structure of Ric-8 proteins and the expected locations of protease-susceptible residues following the α-helical crescent core. For analysis purposes, we subdivided Ric-8B into three regions: domain 1 (residues 1–295) was defined as the first six ARM/HEAT repeats and the first α-helix of the seventh repeat that interacts with the Gα α5 helix and C-terminus; domain 2 (residues 296–455) consists of the remainder of ARM repeat 7 and the three ARM/HEAT repeats that interact with the core of the Gα Ras-like domain (RLD); and the remaining resolved portion of the Ric-8B C-terminal region (residues 456–518) forming the CLH structure that wraps around the Gα RLD to engage Gα Switch II (Figure 1E).

Functional insights into structural elements required for Ric-8B chaperone activity

We assessed the functional importance of Ric-8B and Gαs/olf residues and elements that make key contacts using a cell-based Gαolf protein folding sensor that was introduced into a new CRISPR/Cas9-generated *RIC-8B*$^{-/-}$ HEK293T cell line (Figure 2, Figure S3). Our *RIC-8B* knockout cell line had diminished abundances of endogenous Gαs isoforms, $G\alpha s_{Long}$ and $G\alpha s_{short}$, due to protein misfolding, consistent with results obtained in prior *Ric-8B*-deleted cell line and mouse models[12,29] (Figure 2A). The abundances of other G proteins, including Gαq and total Gβ, were minimally impacted by *RIC-8B* deletion (Figures S3 and S4), verifying the known specificity of Ric-8B for the Gαs/olf class.[9] A previously constructed Gαolf fusion protein with a *Renilla* luciferase (RLuc) module located internally at Gαolf position Gly69[37] was expressed in the *RIC-8B* knockout cell line. The

baseline luminescence signal from these cells was dim but was enhanced markedly by transfection of Ric-8B cDNA (Figures 2B and 2C). We inferred that folding of the internal RLuc module depended on proper Gαolf folding, which is Ric-8B-dependent. A series of Ric-8B point mutants or small deletion mutants were generated to evaluate the importance of contact points with Gαolf. The mutants were co-transfected with the Gαolf-RLuc sensor in the *RIC-8B* knockout cell line, and Ric-8B mutant protein levels were assessed by Western Blot analysis (Figures 2C and S4).

Relative orientation of Ric-8 domains influences Gα substrate specificity

Despite common structural elements (*i.e.,* the Ric-8 ARM/HEAT repeat core and the CLH), the Ric-8B / Gαs/olf complex structures reveal distinct differences in the relative orientation of Domains 1 and 2 when compared to the Ric-8A/G protein complexes, with RMSD values of 2.564Å and 2.587Å between Ric-8B/Gαs and Ric-8A/Gαq or Ric-8A/Gαi_1, respectively. In comparison to Ric-8A, Ric-8B includes an extra 26 amino acid stretch after Glu303 that was not resolved in our structures, located between the first two α-helices of the seventh α-helical (ARM) repeat. This disordered loop appears to be dispensable, as expression of a Ric-8B Δ304–329 construct supported full folding of the Gαolf sensor (Figure 2C). The positioning of Ric-8A and Ric-8B α-helical repeats HEAT1 and HEAT2 are rotated off-axis relative to one another, and by extension, the cognate Gα RLDs are also shifted (Figure S5). In guanine nucleotide-bound Gαs, the face of the Gαs β-sheet, including β strands 4–6, contact the Gαs/olf α5 helix (PDB: 6EG8), whereas in Ric-8B or GPCR-bound Gαs/olf[3] the α5 helix is markedly displaced. In its place, hydrophobic interactions form between the RLD β-sheet and the 9th α-helical repeat of Ric-8B. We examined Ric-8B engagement of the Gαs/olf β-sheet region through tryptophan substitution of two residues within the HEAT9 repeat, Ala449 and Ala453 (Figs. 2C, 2F). A significant decrease in Gαolf sensor folding was observed upon Ric-8B A449W expression (36% of WT Ric-8B) suggesting the importance of Ric-8B α-helix 9b proximity to Gαs/olf β4-β6 (Figure 2C). Interestingly, the Ric-8B A453W mutation had no effect on Gαolf folding, while the equivalent mutation within Ric-8A (A420W) reduced Gαq folding by 90%,[33] illustrating the difference in α-helical repeat (HEAT 9) positioning between the Ric-8 isoforms. Ric-8 isoform differences also manifest in the positioning of the eighth helical repeat (ARM 8), in which Ric-8B E400A disrupted Gαolf folding (32% of WT Ric-8B) while the equivalent Ric-8A mutation (E367A) retained full ability to fold Gαq (Figure 2C).[33]

Ric-8B interactions with Gα α5 helix are required for chaperone activity

The changes of the Gα α5 helix and its engagement by Ric-8 was established through biochemical experiments, and more recently, in the Ric-8A/Gα complex structures.[33,36,38] Ric-8B and Ric-8A bind the C-termini and α5 helices of Gαs/Gαolf and Gαi_1/Gαq, respectively. Interaction of Ric-8B Arg71, Arg75 and Asn123 stabilize the C-terminal end of the α5 helix through side chain hydrogen bonds with the free carboxylate of the final Gαs/olf leucine residue (Fig 2E). Charge reversal mutations, R71E (29% of WT Ric-8B) and R75E (2% of WT Ric-8B), disrupted this critical interaction in the Gαolf sensor folding assay while an alanine substitution at position 123 (N123A, 8% of WT Ric-8B) disrupted a side chain contact to the amide backbone located between the final two conserved leucine residues of Gαs/olf (Figure 2E). To address the potential concern that altered expression of

Ric-8B point mutants might account for the observations of Gαolf sensor misfolding, we conducted a Ric-8B construct expression titration study. Increasing amounts of transfected cDNA of two Ric-8B point mutants that were most deficient in facilitating Gαolf folding (R75E and N123A) only elevated Gαolf sensor luminescence values to ~25% of wild type Ric-8B despite saturated protein production, indicating that dysfunction of the mutated residues accounts for the Gαolf folding defects (Figure S4).

Two additional Ric-8B contacts mediate interactions with the Gαs/olf C-terminus; Ric-8B Phe126 sterically impedes the movement of the Gαs/olf Tyr377/378 to help coordinate the Gα C-terminus. Ric-8B F126A expression modestly reduced Gαolf sensor folding by 20%, supporting the beneficial packing interactions of the hydrophobic residues located in Ric-8B ARM3 and the pi-pi aromatic interaction with Gαs/olf Tyr377/378 (Figure 2C). Arg166 within Ric-8B ARM4 makes a cation-pi contact with Gαs/olf Tyr377/378 and H-bonds to the adjacent Glu378/379-Leu379/380 peptide backbone. A Ric-8B R166A substitution mitigated both interactions and caused a 59% decrease in Gαolf sensor folding. Ric-8B ARM4 residue Phe163 was examined for potential interactions with the Gαs/olf C-terminus. However, the F163A mutant expression did not affect Gαolf sensor folding indicating that the Gαs/olf C-terminus is primarily contacted by HEAT2 and ARM3 repeats of Ric-8B.

The Ric-8B α5 helix binding pocket purveys promiscuity in binding Gα C-termini

Despite the conservation of select Ric-8A and Ric-8B residues that interact with the C-termini of different Gα subunits, we observed differences in the orientations of the Gαi and Gαq or Gαs/olf α5 helices and the electrostatic environment of the α5 helix binding pockets within Ric-8A or Ric-8B domain 1 (Figures 3, 4, and S5). When the structures are aligned through Ric-8 domain 1, there is an angular difference of 18.2° (Ric-8A / Gαi) and 11° (Ric-8A / Gαq) in the orientation of the α5 helix bound within the concave Ric-8 cavity as compared to the Ric-8B / Gαs complex (Figure S5A–E). Comparatively, there is only a 3.4° difference in the equivalent measurement between the Ric-8B/Gαs and Ric-8B/Gαolf complexes. The contacts between Ric-8A and Gαi or Gαq are markedly distinct from the interactions of Ric-8B with Gαs or Gαolf, largely due to the hydrophilic environment of the Ric-8B α5 helix binding pocket, compared to the more hydrophobic pocket of Ric-8A (Figure 4). The differential positioning of the Gα α5 helix binding pockets and the unique chemical environments result in distinct primary contacts between Gα subunits and Ric-8A or Ric-8B. Besides electrostatic differences in the Ric-8 α5 helix binding cavities, there is a notable distinction in spatial volume between Ric-8A and Ric-8B (Figure S5F–G). The cavity of Ric-8B provides an extra ~840 $Å^3$ of space to accommodate the bulkier residues of the Gαs/Gαolf α5 helix. To further investigate the contribution of the α5 helix to the specificity of Gα binding to Ric-8A and Ric-8B, we tested 18-mer synthetic peptides modeled after the Gαs/olf and Gα13 C-termini in protein thermal stability assays using an adapted differential scanning fluorimetry (DSF) protocol[31,33] with purified Ric-8A and Ric-8B (Figure 4B–C). Equivalent peptides modeled after Gαq and $Gαi_1$ were sparingly soluble and intractable for these analyses. For Gαs/olf and Gα13 C-termini we observed that each peptide induced a concentration-dependent thermal stability shift that was specific to its cognate Ric-8 chaperone. The Gαs/olf peptide only stabilized Ric-8B, inducing a maximal 3.3 °C thermal shift, while the Gα13 peptide induced a thermal shift for Ric-8A of 3.6

°C (Figure 4B–C). Several binding studies have examined the effects of sequence swaps within the Gα α5 helix for GPCR coupling[39,40] and binding to Ric-8A,[31,36] but there was no information comparing Ric-8B and Ric-8A in this regard. We therefore tested the effect of swapping the four C-terminal amino acids of both synthetic peptides. Interestingly, the Gαs/13 chimeric peptide that had four C-terminal Gα13 residues imparted a large 4.8 °C stabilizing shift in Ric-8B melting, 1.5 °C more than the WT Gαs peptide. The same peptide did not induce a thermal shift for Ric-8A, indicating that the large and hydrophilic Gαs α5 helix might not fit or bind productively to the more hydrophobic Ric-8A binding pocket (Figure 4B–C). The reciprocal Gα13/s chimeric peptide that had four C-terminal Gαs residues weakly stabilized both chaperones, with a reduced Ric-8A and increased Ric-8B thermal shift in comparison to the WT Gα13 peptide. Collectively, the results suggest that the larger α5-helix binding cavity of Ric-8B can accommodate greater sequence diversity than Ric-8A, which only demonstrated binding to peptides comprised predominantly of Gα13-based residues.

Our structural analysis and protein thermal stability results demonstrate that Ric-8B has the potential to bind the α5 helix of multiple Gα subunit classes, yet it selectively chaperones Gαs/olf in cells, while at high concentrations it can act as a GEF for multiple Gα subunit classes in *in vitro* assays.[9,12,22,25–27] To investigate the influence of the α5 helix on Ric-8 specificity within the context of the entire Gα subunit, we generated Gαolf-RLuc chimeric folding sensors that incorporated the 18 C-terminal amino acids of Gα13, Gαq, or $G\alpha i_1$ in place of the Gαolf residues to test in our cell-based folding platform. Interestingly, all three chimeras exhibited robust folding by co-expressed Ric-8B (Figure 4D), nearly equal to or greater than the WT Gαolf sensor. Conversely, Ric-8A did not fold the wild type Gαolf sensor above background in *RIC-8A* knockout cells, but Ric-8A expression did result in a 10–20% gain of function for folding the Gαolf/Gα13, /Gαq, and /$G\alpha i_1$ α5 helix chimeras (Figure 4D). This implies that Ric-8A is excluded from folding Gαs, primarily because its α5 helix binding cavity is too small to accommodate this G protein, but it can accommodate the smaller α5 helices of the other Gα subunit classes. With its large α5 helix binding pocket, Ric-8B readily accommodates the α5 helices of all Gα subunits, but relies on additional contact points to purvey high affinity Gαs/olf subunit binding. The tolerance of Gα subunit C-termini for Ric-8B-mediated folding was further demonstrated using a Gαolf-RLuc folding sensor modified to contain a four-alanine residue insertion between the N-terminal 5th and 6th positions of the Gα α5 helix (*i.e.,* Gα-Ins4Ala). This modification extends the α5 helix by one helical turn and can be used to form nucleotide-free G protein / GPCR complexes that are resistant to dissociation by nucleotides.[41,42] Ric-8 is a GEF that has high affinity for nucleotide-free Gα and might also bind Gα-Ins4Ala proteins in a bottleneck complex. However, the mechanism of Ric-8-mediated GEF activity differs from that of GPCRs and Ric-8B provided 115% folding of the Gαolf-RLuc Ins4Ala sensor in comparison to the WT Gαolf-RLuc sensor (Figure S6). This result coincides with the finding that Gα-Ins4Ala proteins were active in cell-based assays where they were likely folded by the assistance of a cognate Ric-8 chaperone.[42] Akin to Ric-8A, Ric-8B also requires a minimal length of Gα C-terminal sequence, as a Gαolf-RLuc sensor with a four amino acid C-terminal deletion was not folded by Ric-8B (Figure S6).[33]

Ancestral Ric-8 proteins share the ability to accommodate Gα C-terminal sequence diversity with Ric-8B

The ability of Ric-8B to fold Gαolf chimeras with C-terminal sequences from all four Gα subunit classes resembles the probable chaperoning responsibilities of ancestral Ric-8 proteins such as those found in *D. melanogaster* (*Dm*Ric-8) and *C. elegans* (*Ce*Ric-8). These organisms only express a single *Ric-8* gene which has been shown to regulate signaling outputs contributed by all Gα subunit classes.[16,18,19,24] *Dm*Ric-8 and *Ce*Ric-8 likely participate in the folding of all Gα subunits and are predicted to share structural characteristics with the α5-helix binding cavity of Ric-8B (Figure S5H, AlphaFold AF-Q9W358-F1 and AF-Q9GSX9-F1[43]). We demonstrated the broad chaperoning specificities of *Dm*Ric-8 and *Ce*Ric-8 by detecting measurable folding of Gαolf, and the Gαolf/Gα13, /Gαq, and /Gαi1 α5 helix chimeric RLuc folding sensors in the *RIC-8B* knockout cell line (Figure S6). These results indicate that like Ric-8B, *Dm*Ric-8 and *Ce*Ric-8 accommodate considerable sequence diversity at the α5 helix. We also verified the broad Gα subunit specificities of *Dm*Ric-8 and *Ce*Ric-8 by showing that expression of either gene partially rescued the reduced endogenous Gαs and Gαq levels in mammalian *RIC-8B*$^{-/-}$ or *RIC-8A*$^{-/-}$ knockout cells, respectively (Figure S6).

Gα Switch II and extended proline-rich loop are necessary for folding by Ric-8B

Additional structural determinants that mediate Ric-8B specificity were assessed by examining the contribution of Gα Switch II (SwII, Gαs residues 212–226) (Figures 5 and 6).[1–3] Ric-8A cryoEM complex data previously demonstrated that the Ric-8A CLH engages Gαq and $G\alpha i_1$ SwII and the α3 helix.[32,33] This interaction is thought to help maintain the nucleotide-free, open conformation of Gα subunits to permit subsequent GTP binding, and Ric-8 chaperone dissociation. C-terminal truncations of Ric-8A disrupted Gαi/q/13 subunit folding.[34,44] We observed a similar extension of the Ric-8B CLH adjacent to Gαs/olf SwII (Figures 5, S2, and S7). Implementing cryoSPARC's 3D variability analysis,[45] a tool that helps identify regions of compositional and conformational variability, we discerned the relative stability of the Ric-8B CLH/Gα RLD interaction across the particle set (Figures 5 and S7A, Movie S1). Within a cluster analysis of the 3D variability, using a tight mask, the particle set was partitioned into five discrete classes. We observed that structuring of the Ric-8B CLH α-helix correlated with increased cryoEM density ordering of Gα Switch II. Furthermore, as the Ric-8B CLH α-helix density appeared destabilized in select particle classes, residues within the Gαs RLD β3 strand (*i.e.,* Asn204 and Phe205) were found to be in closer proximity to α-helix 9b of the final HEAT repeat (residues 449–455) within the Ric-8B core. Loose masking and expansion of our cleaned particle set to include semi-cleaned particles, not contributing to our high-resolution structures, enabled the capture of low-resolution reconstructions that displayed density corresponding to what appears to be the C-terminus of Ric-8 and the Gα alpha helical domain (Figure S7B–C). Although the reconstructions only represent a sub-population of particles within the data set, they provide approximations of the locations of these flexible domains relative to the core regions of the Ric-8B/Gα complexes that were resolved in near-atomic detail.

We next measured the influence of Gα SwII for Ric-8 specificity by creating Gαolf-RLuc sensor chimeras with Gα13, Gαq, and $G\alpha i_1$ SwII sequence substitutions. Ric-8B testing

uncovered a substantial decrease in protein folding (50%) of the Gαolf/13 SwII chimeric sensor and a minor decrease in Gαolf/i_1 SwII (88% of Gαolf) sensor folding (Figure 6). Ric-8B folding of the Gαolf/q SwII chimeric sensor was elevated modestly relative to the Gαolf sensor. In sum, these observations indicate that the Gα SwII is necessary for efficient Ric-8B binding to Gα subunits and that interactions of Ile221/2 and Gln222/3 of Gαs/olf SwII with the Ric-8B CLH are preferred contact points, whereas equivalent bulkier (Phe220) and negatively charged (Glu221) residues of Gα13 might abrogate a Ric-8B/Gα13 interaction. Ric-8A testing with the Gαolf-Gα SwII chimeras did not produce luminescent sensor signals over negative control values (Figure 6C), emphasizing the incompatibility of the Gαs/olf α5 helix for binding to Ric-8A.

Since replacement of the SwII and α5 regions of Gαolf with those of Gαq still resulted in sensor folding by Ric-8B, we postulated that an extended twelve residue loop within Gαs/olf located between the αG and the α4 helices (αG-α4 loop, Gαolf residues 312–323) may help impart Gαs/olf specificity for Ric-8B (Figure 7). This highly charged, proline-rich loop contacts the ARM7 repeat of Ric-8B (Figure 7A–B) but is not present in Ric-8A-client Gα subunits. We reasoned that the angular differences of the Gα α5 helix and altered axis of the RLD (β4-β6 region) observed in our Ric-8B complexes, relative to Ric-8A, were influenced by this unique Ric-8B–Gαs/olf interaction contact point (Figure S5). To assess its significance, we designed and tested Gαolf folding sensors with internal deletions of the αG-α4 loop (Δ312–318) as well as the loop and α4 helix (Δ312–323) (Figure 7C). Gαolf-RLuc Δ312–318 and Δ312–323 truncations displayed dramatic Ric-8B-dependent declines in folding of 44% and 63%, respectively in comparison to the WT Gαolf sensor (Figure 7C). The αG-α4 loop primarily contacts Ric-8B through weak backbone interactions rather than side chain specific contacts. We next introduced these Gαolf αG-α4 loop truncations into our α5 helix chimeras (Gαolf/13, Gαolf/q, Gαolf/i1) with the intent to generate Ric-8A-capable, Gα sensor chaperoning substrates. Ric-8A did not experience the same αG-α4 loop requirement for folding of Gαolf chimeric sensors (Figure 7C). Ric-8A consistently folded Gαolf/13, Gαolf/q, and Gαolf/i_1 α5-helix chimeras containing either deletion (Δ312–318 or Δ312–323) at ~10–20% folding relative to wild type Ric-8B folding of the Gαolf sensor. The Ric-8B/Gαs and Ric-8B/Gαolf cryoEM complex structures both show that the αG-α4 loop interacts with the 7B-7C loop of the ARM7 repeat of Ric-8B (Figure 7A–B). Ric-8B ARM7 loop replacement with that of Ric-8A, however, produced only a minor 10% decrease in chaperoning function (Figure S6). The complementary Ric-8A ARM7 loop sequence swap to Ric-8B did not generate Gαolf sensor gain-of-function folding, suggesting that this interface primarily regulates Gαs/olf folding by Ric-8B with only a minor contribution towards Ric-8 isoform selectivity.

Discussion

Here we determined the structures of the molecular chaperone Ric-8B in complex with its client proteins $Gαs_{short}$ and Gαolf. An outcome of our work has been to distinguish Ric-8A and Ric-8B features that impart specificity for folding client G proteins. In addition, we describe the structure of Gαolf, a historically challenging protein to purify that had evaded structure determination. We found that Ric-8B binds to an open, nucleotide-free conformation of $Gαs_{short}$ and Gαolf through contacts with multiple areas of the RLDs of the

G proteins. This includes a unique interaction of the Ric-8B ARM repeat 7 with the extra i3 insertion that is contained within the αG-α4 loop of Gαs/olf, an interaction of the Ric-8B CLH with Gα Switch II, and an interaction of the Ric-8B ARM/HEAT repeat core with the outwardly rotated and translated α5 helix and C-termini of the Gα subunits.

The chaperoning ability of Ric-8B was compromised by internal truncations that eliminated the i3 insertion of the Gαolf αG-α4 loop, yet there was no gain of function for Ric-8A in folding i3 Gαolf truncations (Figure 7C). This has some parallels to prior work that identified the Gαs αG-i3-α4 loop as an element required for adenylyl cyclase (AC) activation.[46,47] However, placement of the Gαs i3 insertion within Gαi, created a chimera that failed to activate AC,[48] prompting additional work that found that multiple Gαs structural features contribute to AC activation.

Mutations of key Ric-8B residues within domain 1 (ARM/HEAT repeats 1–6) that interact with the α5 helix disrupted Gαolf folding in cells, consistent with prior Ric-8A-[31,36] and GPCR-[39,40] based findings that identified the Gα C-terminus as a critical recognition element (Figure 2). Although Ric-8B adopts an overall ARM/HEAT repeat architecture that is similar to Ric-8A,[32–34] the positioning and electrostatic interactions of the Gα subunit α5 helix with these two chaperones is distinct. The significantly larger and more hydrophilic nature of the Ric-8B α5 helix binding cavity permits greater latitude for accommodating Gα subunit C-terminus diversity when compared to Ric-8A. Ric-8A seemingly cannot accommodate the bulky Gαs/olf α5 helix side chains, while Ric-8B readily binds to these sterically larger C-terminal residues as well as smaller (Gα13, Gαq, $G\alpha i_1$ classes) ones.

The larger α5 helix binding cavity of Ric-8B contributing to Gαs/olf specificity parallels recent studies on the requirements for G protein coupling to GPCRs. The Gα C-terminus and α5 helix are a primary interaction point with GPCRs binding within a cytosolic cavity of the 7TM bundle that is formed by the outward movement of transmembrane helix 6 (TM6) upon activation of most receptors. The extent of opening of the TM6 cytoplasmic half defines the size of the C-terminus/α5 binding cavity of GPCRs and is generally larger in Gs-coupled receptors compared to Gi-coupled GPCRs. This has led to the hypothesis that receptor G protein specificity is, in part, dictated by the ability to accommodate the bulkier residues of Gαs.[3,49–52] The loose binding requirements of the large Ric-8B α5 helix binding cavity presents an opportunity to identify pharmacophores that may disrupt endogenous Gα subunit folding. Our Ric-8B protein thermal stability assay and cell-based Gαolf folding sensor might be utilized to identify negative regulators that specifically bind to Ric-8B over Ric-8A and serve as potential therapeutics to combat mutant Gαs/olf overactivity, including targeting $G\alpha s_{long}$, which is misregulated in ~4% of all cancers[53] and was recently identified as a contributor to myelodysplastic syndrome through inappropriate activation of ERK/MAPK signaling.[54] Ideally these ligands could be tuned to disrupt specific Ric-8B/Gαs folding interactions and the overall screening methodology could be applied to parse ligands that modulate Ric-8A-dependent G protein folding.

Ric-8 binding to the Gα subunit α5 helix alone does not determine specificity. Gα SwII is another major Ric-8 recognition element, but unlike the α5 helix it is not directly bound by GPCRs.[3] Gα SwII when bound to Ric-8B appeared to be dynamic as it exhibited

conformational variability evidenced by our cryoEM analysis (Figures 5, 6, and S7). Results from chimeric protein Gαolf folding sensor corroborated its importance, as Ric-8B folding activity was compromised when Gα13 SwII was swapped into the Gαolf sensor (Figure 6C). Further support that efficient Gα folding requires SwII interactions with Ric-8 proteins, specifically by the CLH, comes from previous data demonstrating the greatly impaired interaction strengths of Gαolf or Gαs with an alternatively spliced Ric-8B product that lacks exon 9 (Ric-8BΔ9).[9,15,25] Ric-8BΔ9 lacks residues 483–524, which essentially constitutes a natural internal deletion of the CLH (residues 484–518) as observed in the structures.

An important aspect that remains to be characterized is the impact that the Ric-8 C-terminus has in moderating Gα subunit folding. Like Ric-8A, the C-terminus of Ric-8B (residues 516–560) was unresolved in the Gα complex structures, yet it is required in cells for Gα subunit folding. Expression of C-terminally-truncated Ric-8A (Ric-8A-ΔCT, residues 1–492 of 530) which includes its full CLH, did not rescue the Gαq abundance defect of *RIC-8A*$^{-/-}$ cells,[44] and the protein did not support folding of a $G\alpha i_1$-GFP sensor in cell-free extracts.[34] However, its capacity to serve as a GEF for $G\alpha i_1$ and Gαq *in vitro* exceeded full length Ric-8A.[34,36] The reasons for this remain unclear, but we hypothesize that the unresolved Ric-8 C-terminus may serve to briefly keep the Gα AHD separated from the RLD in pre-folded Gα subunits until the time that the G protein adopts its near final fold and is competent to productively bind GTP. In situations where Ric-8 proteins are absent, for example, in gene-deleted cells or when attempting to produce recombinant Gαq in *E. coli*, the AHD would not be blocked from rapidly binding to the RLD and this may cause the G protein to adopt a bottleneck (mis)fold that is nucleotide-free and incapable of undergoing nucleotide exchange or activation. Indeed, much recombinant, soluble Gαq can be produced in *E. coli*, but the protein is not functional, a term previously described by Paul Sternweis and colleagues as comatose Gα.[55,56] In *in vitro* GEF assays, the Ric-8 substrate is not pre-folded, nucleotide-free Gα, but functionally folded Gα-GDP. It may be that Ric-8 truncated proteins that lack the C-terminus are more efficient at disrupting the already folded Gα structure to insert the CLH alongside SwII and disrupt nucleotide binding elements to initiate rapid GDP release. The proposed function of the C-terminus to pause AHD and RLD association would not be necessary for Ric-8 to facilitate GDP/GTP exchange *in vitro*.

STAR★Methods

Resource Availability

Lead Contact—Further information and requests for resources and reagents should be directed to and will be fulfilled by the lead contact, Gregory G. Tall (gregtall@med.umich.edu)

Materials Availability—All unique/stable reagents generated in this study are available from the lead contact upon request.

Data and Code Availability—The MS proteomics data have been deposited to the ProteomeXchange Consortium (http://proteomecentral.proteomexchange.org) through the PRIDE partner repository with the data set identifier: PXD036645.[57]

CryoEM maps of Ric-8B in complex with Gαs and Gαolf have been deposited in the Electron Microscopy Data Bank under accession codes EMD-28223 and EMD-28224, respectively.

The atomic coordinates of Ric-8B in complex with Gαs or Gαolf have been deposited in the Protein Data Bank under the accession codes 8EL7 and 8EL8, respectively.

This paper does not report any original code.

Any additional information required to reanalyze the data reported in this paper is available from the lead contact upon request.

Experimental Model and Subject Details

HEK293T cells were unauthenticated and purchased from the American Type Culture Collection (ATCC), catalog number, CRL-3216. Maximum efficiency DH5α bacteria were unauthenticated and purchased from ThermoFisher, catalog number 18258012. Rosetta 2 (DE3) pLysS bacteria were unauthenticated purchased from Novagen, catalog number 71397. DH10Bac bacteria were unauthenticated and purchased from ThermoFisher, catalog number 10361012. *Sf*9 cells were unauthenticated and purchased from Expression Systems, catalog number, 94–001F.

Method Details

Antibodies—Rabbit polyclonal antiserum 2413 (used at 1:5000) against Ric-8B and 1184 (used at 1:10,000) against Ric-8A were described previously.[12,22] G protein subunit antiserum was used to detect Gβ1–4 (used at 1:10,000) (B600).[56] Commercial IgG purified polyclonal antibodies for Gαs (Sigma-Millipore) (used at 1:2000), and Gαq/11 (Sigma-Millipore) (used at 1:2500) were utilized for measuring G protein abundance. A commercial IgG purified monoclonal antibody for was used to detect GAPDH (Invitrogen, ZG003) for loading controls. Primary antibodies for phospho-site detection were described previously.[34] Briefly, the Phospho-CK2 Substrate [(pS/pT)DXE] MultiMab™ Rabbit mAb mix (#8738, Cell Signaling Technology) was used to detect pThr473 in Ric-8B (pThr440 in Ric-8A). The enriched IgG fraction of rabbit antiserum (6383) specifically detects pSer468 in Ric-8B (pSer435 in Ric-8A).[34]

Phos-tag SDS-PAGE—This method is described in Yu *et al.*[35] and adapted from English *et al.*[58] Protein samples were exchanged into a chelator-free buffer (20 mM HEPES pH 8.0, 50 mM NaCl) using Cytiva PD-25 centrifugal buffer exchange columns. After measuring protein concentrations via Bradford assay and diluting appropriately, samples were mixed 1:1 with 2x Phos-tag Sample Buffer (0.1% w/v bromophenol blue, 2% w/v SDS, 20% v/v glycerol, 0.5 M Tris-HCl pH 8.5, 0.2 M DTT) and heated at 95°C for 5 min. Phos-tag gels were cast fresh, resolving gel (8% 29:1 acrylamide/bis-acrylamide (Bio-Rad), 350 mM bis-tris pH 6.8, 75 μM Phos-tag reagent (Wako Chemical Industries), 150 μM $Zn(NO_3)_2$, 0.1% v/v tetramethylethylenediamine (TEMED), 0.05% w/v ammonium persulfate (APS)) was layered with isopropanol and allowed to polymerize for ~40 min before being rinsed with water and overlaid with stacking gel (4% 29:1 acrylamide/bis-acrylamide, 350 mM bis-tris pH 6.8, 0.05% w/v APS, 0.1% v/v TEMED), which was allowed to polymerize for

~1 h. Running buffer (50 mM Tris-HCl pH 7.8, 50 mM MOPS, 0.1% w/v SDS, and 5 mM sodium bisulfite) was used for flushing out wells and samples were immediately loaded. Gels were run submerged in running buffer with freshly added 5 mM sodium bisulfite at 100 V for 3.5–4 h. Gels were visualized using Coomassie Blue staining.

Membrane and cytosol preparation—Wild-type, *RIC8A*$^{-/-}$, *RIC8B*$^{-/-}$ or *RIC8A*$^{-/-}$;*RIC8B*$^{-/-}$ knockout HEK293T cells were washed and harvested in PBS containing a protease inhibitor (PI) cocktail (23 mg/mL phenylmethylsulfonyl fluoride, 21 mg/mL Na-*p*-tosyl-L-lysine-chloromethyl ketone, 21 mg/mL L-1-*p*-tosylamino-2-phenylethyl-chloromethyl ketone, 3.3 mg/mL leupeptin, and 3.3 mg/mL lima bean trypsin inhibitor) and 1 mM dithiothreitol (DTT). Cells were suspended in phosphate buffered saline (PBS) with PI and DTT and lysed using a nitrogen cavitation device (Parr Industries). The lysates were centrifuged at 1000 g for 10 min at 4°C, and the supernatants were further centrifuged at 100,000 g at 4°C for 40 min. The supernatant was carefully removed and isolated as the cytosolic fraction prior to storage. The remaining membrane pellet was homogenized in PBS with PI and DTT before −80°C storage. The total protein content of cytosol and membrane samples was measured by Bradford assay, and each sample was diluted to 1X in SDS reducing sample buffer and heated at 95°C for 5 min prior to 12% SDS-PAGE resolution using 20 μg total protein per lane.

Immunoblotting—All gels were transferred onto nitrocellulose membranes, blocked in 5% (w/v) milk in BLOTTO (TBS and 0.1% NP-40) and immunoblotted at 4°C overnight with the antibodies listed above. Membranes were washed with TBST, incubated with 1:5000 IR-800 donkey anti-rabbit or anti-mouse antibody (LI-COR) in 5% (w/v) milk in BLOTTO for 1 hr at room temperature. After incubation, membranes were washed twice in TBST, twice in TBS, and imaged using an Invitrogen iBright system. Western Blot lanes were quantified via pixel densitometry using Adobe Photoshop.

Purification and in vitro phosphorylation of Ric-8B—Recombinant GST-TEV-Ric-8B (~20 mg) was purified from High-Five insect cells and the fusion protein was cleaved with 0.85 mg of purified, enhanced TEV protease in 10 mL of 20 mM HEPES pH 8.0, 50 mM NaCl, 1 mM EDTA, 1 mM DTT and PI for 1.5 h at 22°C.[9,59] The TEV cleavage reaction was incubated with 75 μL of Protein Kinase CK2 holoenzyme (NEB), 3 mM ATP pH 8.0, 25 mM HEPES pH 8.0, 100 mM NaCl, 1 mM EGTA, 10 mM $MgCl_2$, 1 mM DTT and PI in a 25 mL reaction at 25 °C for 1.5 hr and at 30 °C for an additional 30 min.[35] The kinase reaction was brought to 50 mL with Buffer A (20 mM HEPES pH 8.0, 100 mM NaCl, 1 mM EDTA, 1 mM DTT), filtered through a 0.2 μm syringe filter and loaded onto a Mono Q 10/100 column (Cytiva) equilibrated with Buffer A. Phosphorylated Ric-8B was eluted with a linear gradient of increasing NaCl concentration. Fractions containing phosphorylated Ric-8B were pooled and stored at −80°C. The procedure typically yielded ~3 mL of 1.0 – 1.5 mg/mL phosphorylated Ric-8B.

Recombinant Ric-8B was also purified from Rosetta 2 *E. coli* transformed with pET21a GST-TEV-Ric-8B.[9] Transformants were cultured in 3 mL LB carbenicillin over day cultures, then used to inoculate overnight 150 mL cultures. The cells were pelleted by centrifugation and resuspended in 15L of LB carbenicillin. Cells were grown to an $O.D._{600}$ of 0.6 and

cooled for 1.5 h at 4°C until the cultures were ~16°C. Protein production was induced at 16°C with 30 μM Isopropyl β-D-1-thiogalactopyranoside (IPTG) in an orbital shaker set to 175 rpm for 20 h. Cells were harvested via centrifugation for 10 min at 8000 xg and frozen with liquid nitrogen. Frozen cells were thawed into 350 mL lysis buffer (20 mM HEPES pH 8.0, 150 mM NaCl, 1 mM DTT, 5 mM EDTA, and protease inhibitor cocktail) and stirred with 400 mg chicken egg-white lysozyme (Sigma) at 4°C for 40 min. DNAse I (4 mg) and 4 mL of 1M $MgCl_2$ were added and the mixture was stirred for an additional 15 min. The cell lysate was clarified by centrifugation at 10,000 xg for 10 min, followed by centrifugation at 100,000 xg for 40 min. The pellet from the initial 10,000 xg centrifugation was frozen with liquid nitrogen and thawed in an additional 400 mL of lysis buffer. A handheld blender was used for thorough secondary cell lysis. The secondary lysate was clarified by differential centrifugation as described above, and the clarified supernatants from both lysis steps were combined and loaded by gravity onto a 5 mL bed volume glutathione Sepharose 4B column (Cytiva). The column was washed with 50 mL of lysis buffer, and GST-TEV-Ric-8B was eluted with lysis buffer containing 20 mM reduced glutathione. The protein was filtered through a 0.22 μm polyethersulfone syringe filter and loaded onto a MonoQ 10/100 column (Cytiva) equilibrated with 20 mM HEPES pH 8.0, 100 mM NaCl, 1 mM EDTA, 1 mM DTT. GST-Ric-8B was eluted with a linear gradient up to 550 mM NaCl and elution fractions were analyzed by SDS-PAGE, pooled, concentrated using a 30,000 MWCO ultracentrifugal device (Amicon), snap frozen with liquid nitrogen, and stored at −80°C. This procedure yielded approximately 4.5 mg of purified GST-Ric-8B per liter of culture.

Purification of $G\alpha s_{short}$ and Gαolf—$G\alpha s_{short}$ and Gαolf were purified using the GST-Ric-8 association method.[28] High-Five insect cells were co-infected with baculoviruses encoding GST-Ric-8B and the desired Gα subunit before being harvested by centrifugation after 48h. Cell were lysed by nitrogen cavitation in 300 mL of lysis buffer (20 mM HEPES pH 8.0, 150 mM NaCl, 1 mM DTT, 1 mM EDTA, 0.05% (w/v) Genapol C100 detergent, and protease inhibitor cocktail. The lysate was clarified via sequential centrifugation at 3000 xg for 10 min and 100,000 xg for 45 min. The supernatants were loaded over a packed 5 mL glutathione Sepharose 4B column (Cytiva). The column was washed with 100 mL wash buffer (20 mM HEPES pH 8.0, 100 mM NaCl, 1 mM DTT, 11 mM CHAPS and protease inhibitor cocktail) and warmed to 22°C. Gα subunits were eluted with 20 mM HEPES pH 8.0, 100 mM NaCl, 1 mM DTT, 10 mM NaF, 30 μM $AlCl_3$, 11 mM CHAPS, 100 μM GDP, concentrated in 30,000 MWCO ultracentrifugal device and gel filtered over tandem Superdex 75 and 200 10/300 GL columns (Cytiva) in gel filtration buffer (20 mM HEPES pH 8.0, 1 mM DTT, 0.5 mM EDTA, 1 μM GDP, 11mM CHAPS). Fractions containing Gα were pooled, concentrated, snap frozen in liquid nitrogen, and stored at −80°C.

Ric-8B and Gα complex assembly—Phosphorylated Ric-8B (4 – 6 mg) was mixed with ~7 mg of purified $G\alpha s_{short}$ or Gαolf and 125 mU apyrase in gel filtration buffer (20 mM HEPES pH 8.0, 100 mM NaCl, 1 mM EDTA, 1 mM DTT). The protein mixtures were incubated at 22°C for 30 min and then concentrated to ~5 mL using a 50,000 MWCO Amicon ultra centrifugal concentration device. Ric-8B/Gα complexes (~105 kDa) were separated from excess Gα (~45 kDa) using a Superose 6 16/60 column that was resolved with gel filtration buffer. Column fractions were analyzed by Coomassie-stained SDS-PAGE

to identify the Ric-8B/Gα complex pool. The pool was concentrated using a 30,000 MWCO ultracentrifugal device (Amicon). These procedures yielded ~2.5–3.0 mL of 1.2 mg/mL Ric-8B:Gαs complex and approximately ~0.7 mL of 2.6 mg/mL Ric-8B Gαolf complex. Complexes were further concentrated to 3.3–3.5 mg/mL and analyzed by negative stain transmission electron microscopy to ensure sample quality immediately before freezing on cryoEM grids.

Mass spectrometry—Purified Ric-8B protein (10 μg) was reduced with 15 mM DTT at 37°C for 30 min, followed by alkylation with 15 mM iodoacetamide at 37°C for 45 min. The protein was then digested with sequencing-grade trypsin or chymotrypsin (Promega) at 37°C for 45 min. The protease/Ric-8B ratio was 1:20. Digestion was quenched with formic acid, and samples were desalted using a Waters HLB solid-phase extraction plate. The eluted samples were lyophilized and resuspended in 0.1% w/v TFA prior to analysis. Each digested sample (1 μg) was analyzed by nano LC-MS/MS with a Waters M-Class HPLC system interfaced to a ThermoFisher Fusion Lumos mass spectrometer. Peptides were loaded on a trapping column and eluted over a 75-μm analytical column at 250 nL/min packed with Luna C18 resin (Phenomenex). The mass spectrometer was operated in data-dependent mode, with the Orbitrap operating at 60,000 FWHM and 15,000 FWHM for MS and MS/MS, respectively. The instrument was run with a 3s cycle for MS and MS/MS. Data were searched using a local copy of Mascot (Matrix Science). Mascot files were parsed into Scaffold (Proteome Software) for validation, filtering, and creating a non-redundant list per sample. Data were filtered using a 1% protein and peptide false discovery rate (FDR) and requiring at least two unique peptides per protein to confirm specific peptide phosphorylation sites.

Peptide-binding thermal shift assay—C-terminally amidated peptides comprising the last 18 residues of Gα13 and Gαs, along with chimeric peptides transposing the last five residues of each, were synthesized and purified by HPLC (Genscript). Peptides were prepared as 50 mM stock solutions in anhydrous DMSO. Purified Ric-8B proteins (1 mg/mL) were exchanged into thermal shift assay buffer (20 mM HEPES pH 7.4, 140 mM KCl, 5% v/v glycerol, 1 mM DTT) based on previously characterized Ric-8 studies.[31,33] SYPRO Orange dye provided as a 5000X concentrated dye solution in DMSO (Sigma) was diluted to a 10X concentrated stock into the diluted protein to create a 2X protein/dye mix. Peptide stocks were prepared by serially diluting the 50 mM DMSO stocks into thermal shift assay buffer at twice the desired assay concentration. Protein/dye mix (10 μl) was aliquoted into wells of MicroAmp Optical 384-well qPCR plates (Applied Biosystems), and 10 μl of the 2X peptide dilutions were added so that each well contained 0.15 mg/ml protein, 5X dye (relative to manufacturer intended concentration for gel staining), and the desired final concentration of peptide. Plates were centrifuged at 500 xg for 3 min and covered with optical adhesive film (VWR). Melt assays were performed in an Applied Biosystems QuantStudio 7 using a DNA melt curve setting modified such that following incubation at 25°C for 2 min, the temperature was increased using a 0.5°C, 30 s step gradient until a final 2 min hold at 75°C, while obtaining readings using the x1 and m4 filters.

Cloning and Ric-8 expression constructs—Mouse Ric-8B cDNA (Invitrogen, LLAM collection, clone 6490136) was amplified by linker-based PCR with *Bam*HI and *Sal*I sites and subcloned into the *Bam*HI and *Xho*I sites of pcDNA3.1. The same Ric-8B cDNA was also subcloned into pFastBac-1 with an N-term GST-TEV tag.[11] Rat Ric-8A cDNA was amplified by linker-based PCR and subcloned into the *Eco*RI and *Xho*I sites of pcDNA3.1/hygromycin.[33] *Drosophila melanogaster* Ric-8 (*Dm*Ric-8) was subcloned from pVJL11 by *Eco*RI and *Sal*I restriction enzyme digestion and ligation into the *Eco*RI and *Xho*I sites of pcDNA3.1.[11] *Caenorhabditis elegans* Ric-8 (*Ce*Ric-8) was subcloned from pVJL11 by *Bam*HI and *Sal*I digestion and ligation into the *Bam*HI and *Xho*I sites of pcDNA3.1. QuikChange mutagenesis with PfuTurbo Polymerase (Agilent) was used to produce point mutations and deletions in mouse Ric-8B and human Gαolf RLuc plasmids.[37] All primers used and plasmids generated in this work are listed in Table S3 and Table S4.

RIC-8B-deleted cell lines and the Gαolf-RLuc biosensor protein folding assay —HEK293T cells were cultured in Dulbecco's modified Eagles's medium (DMEM) (Invitrogen) supplemented with 10% (v/v) fetal bovine serum (FBS) (Gibco). *RIC-8B* was deleted from wild type and *RIC-8A* knockout cells[34] using CRISPR technology as described previously[60] by the University of Michigan Human Stem Cell and Gene Editing Core. Briefly, wild type and *RIC-8A*$^{-/-}$ cells were transfected with the *RIC-8B* guide RNA sequence 5'-TGTGACGGTAGACAGTTGGA-3', *Sp*Cas9 protein and ctRNA complex. Cells were then placed into a 24-well culture plate and allowed to recover for two days, followed by clonal cell isolation using two successive 96-well plate serial dilutions.[61] Deletion of *RIC-8B* in clonal cell line outgrowth cultures was confirmed by sequencing of polymerase chain reaction (PCR)-amplified genomic DNA and a *RIC-8B* specific TaqMan Gene Expression assay (Applied Biosystems) (Figure S3).

An optimized Gαolf-*Renilla* luciferase (RLuc) fusion construct was produced by Yano, H. *et. al.*[37] Gαolf folding assays were performed in the *RIC-8B* knockout HEK293T cell line after transient expression of WT or mutant *Ric-8* constructs and the Gαolf-RLuc sensor. *RIC-8B* knockout HEK293T cells in 6-well format were transfected using 5 μl of Lipofectamine2000 and 200 ng of Gαolf-RLuc and 200 ng of WT or mutant *Ric-8* constructs, described in detail above, in 100 μl of Optimem. cDNA titration experiments using WT or mutant (R75E, N123A, A449W) *Ric-8* constructs were performed with 200 ng, 400 ng or 800 ng of Ric-8B plasmid. Total DNA amounts were balanced to 1.6 μg with pcDNA3.1. At 24 h post-transfection, cells were counted and seeded into white, 96-well, TC-treated plates at 40,000 cells per well in 120 μL of Fluorobrite medium (Gibco) containing 10% FBS. At 3 h after cell seeding, the medium was supplemented with 100 μg/mL of cycloheximide (CHX) (Sigma Aldrich) to achieve 200 μL volume per well. At 19 h after CHX treatment, the plates were centrifuged (500 g for 5 min) and 150 μL of medium was removed. Cells were lysed by addition of 50 μL of 2X *Renilla* Luciferase buffer[62] with final assay concentrations of 3 μM coelenterazine H, 5% M-PER (Invitrogen) and 0.2% w/v Triton-X100. Luminescence reads were taken 10 min after cell lysis using a TriStar2 plate reader (Berthold). Data were plotted as normalized percent Gαolf folding values with respect to the assay signal window among transfections with and without WT Ric-8B plasmid.

Fluorescent imaging of Gαolf-mVenus—*RIC-8B* KO HEK293T cells were transiently transfected in 6-well format with Lipofectamine2000 using 200 ng of Gαolf-mVenus and 200 ng of WT Ric-8B or pcDNA3.1.[37] Cells were washed and lifted 24 h after transfection and plated at 50,000 cells per 35 mm dish with a 20 mm glass-bottom (Bioland Scientific) that had been pretreated for 30 min with 100 μg/mL poly-D-lysine (Millipore). Images were acquired using a Leica DMi8 microscope in confocal mode with a 63x oil objective lens using 488-nm excitation for mVenus detection 24 h after seeding.

CryoEM Data Collection—Specimen suitability was first evaluated by negative stain EM [63] which showed monodisperse samples.[64] For cryoEM of the Ric-8B/Gαs complex, 3.5 μL of 3.3 mg/mL sample was applied to glow-discharged UltrAuFoil gold grids (Quantifoil, Au300-R1.2/1.3). The grids were blotted using an FEI Vitrobot Mark IV (ThermoFisher) at 20 °C and 100% humidity and then plunge frozen in liquid ethane. CryoEM imaging was performed on a Titan Krios (ThermoFisher) electron microscope equipped with a K3 Summit direct electron detector (Gatan). The microscope was operated at 300 kV accelerating voltage, with a set magnification of 29,000x in counting mode resulting in a magnified pixel size of 0.8521 Å. Movies were obtained at an exposure rate of 24.2 electrons/ $Å^2$/sec with defocus ranging from −1.8 to −0.8 μm. The total exposure time was 2.497 sec over 50 frames per movie stack. Automatic data acquisition was performed using SerialEM[65] for all data sets. CryoEM grids for the Ric-8B/Gαolf complex, at 3.5 mg/mL, were prepared similarly to the Ric-8B/Gαs complex. Imaging was performed using identical operating conditions, except for differences in exposure settings. Movies were obtained at 27.55 electrons/$Å^2$/sec exposure rate with a total exposure time of 2.49 sec over 55 frames per movie stack.

Image Processing and 3D Reconstruction—Dose-fractionated image stacks were subjected to beam-induced motion correction and dose-weighting using MotionCor2.[66] Contrast transfer function parameters for each non-dose weighted micrograph were determined by CtfFind-4.1.[67] For all data sets; MotionCor2, CtfFind-4.1, autopicking, and extraction were performed in RELION 3.1.[68] For the Ric-8B/Gαs complex, 9,597,316 particles from 9,416 micrographs were extracted using semi-automated particle selection. Subsequently, two rounds of 2D classification and five rounds of 3D classification (coupled *ab initio* and heterogeneous refinement operations) were performed on a binned dataset (pixel size 3.41 Å and 1.70 Å, respectively) using cryoSPARC.[69] A refined set of 707,174 unbinned particles (0.8521 Å/pix) was subjected to homogeneous and non-uniform refinement in cryoSPARC.[70] The data set was exported to RELION for five rounds of 3D classification without alignment, 3D Refinement, and Bayesian Polishing. Homogeneous refinement of the resultant set of 349,857 particles in cryoSPARC produced a final map at a global indicated resolution of 2.8 Å. CryoSPARC's 3D Variability Analysis (3DVA)[45] was used to determine conformational heterogeneity in the final data set, as well as an expanded set of particles (1,021,554 particles) that had been semi-cleaned through 2D and 3D classification and then refined by homogeneous refinement. The former set of particles was processed by 3DVA with three modes, a filter resolution of 7Å, and a tight mask encompassing the resolved regions in the unsharpened final map. "Cluster" mode analysis on the first principal component (PC0) separated the 3DVA results into five

discrete clusters of particles that were further refined individually through homogeneous refinement. Additionally, both sets of particles were processed by 3DVA using a loose mask encompassing the resolved regions and an area adjacent to the complex that was hypothesized to contain the Gαs alpha helical domain. “Cluster” mode analysis on the first principal component (PC0) then separated the 3DVA results into ten discrete cluster maps filtered at a resolution of 10Å.

For the Ric-8B/Gαolf complex, 4,695,512 particles from 4,670 micrographs were extracted using semi-automated particle selection. Two rounds of 2D classification and seven rounds of 3D classification (coupled *ab initio* and heterogeneous refinement) were performed on a binned dataset (pixel size 3.41 Å and 1.70 Å, respectively) using cryoSPARC. Homogeneous refinement of the resultant set of 247,416 unbinned particles (0.8521 Å/pix) produced a final map at a global indicated resolution of 3.2 Å. UCSF Chimera[71] and ChimeraX[72] were used for map/model visualization, using Wiggle[73] interface to aid 3DVA analysis.

Model Building—The initial model for the Ric-8B/$G\alpha s_s$ complex was generated as a homology model from the cryoEM structure of Ric-8A/$G\alpha i_1$ (PDB ID: 6VU8[33]; 61.8% sequence similarity to Ric-8A and 58.7% sequence similarity to $G\alpha i_1$) using SWISS-MODEL.[74] An initial homology model of Ric-8B/Gαolf was generated from the final Ric-8B/$G\alpha s_s$ complex structure reported in this manuscript (PDB ID: 8EL7, 90.3% sequence similarity between $G\alpha s_s$ and Gαolf). Homology models were placed into respective cryoEM maps using the Chimera ‘fit-in-map’ function. Iterative rounds of interactive model adjustment in Coot (version 0.9.2 EL)[75] followed by real-space refinement in Phenix (version 1.17.1–3660)[76] employing secondary structure restraints in addition to the default restraints were performed to improve the modeling.

Structure Comparison—RMSD values were determined using the model align tool in PyMol Molecular Graphics System (Schrödinger). RMSD comparison between Ric-8B:$G\alpha s_s$ (PDB ID: 8EL7) and Ric-8A:Gαq (PDB ID: 6VU5) or Ric-8B:Gαolf (PDB ID: 8EL8) were calculated using 500 to 500 atoms; Ric-8B:$G\alpha s_s$ (PDB ID: 8EL7) and Ric-8A:$G\alpha i_1$ (PDB ID: 6VU8) was calculated using 494 to 492 atoms. Analysis of relative domain positioning was determined using UCSF Chimera.[71] The centers of mass defined centroid positions within the structures for residues 1–295, residues 296–492, and the Ras-like domain of Gα. Alignment was made to the armadillo repeat domain of each structure as that region is highly similar between structures. Axes were defined between centroids and along the Gα α5 helices.

Cavity Volume Calculation—The volume of the Gα α5-helix binding pocket of Ric-8A and Ric-8B was calculated using VMD (version 1.9.3)[77] with the Epock (v.1.0.5) plugin.[78] The sampling area was defined using the cylinder method, with coordinates in x, y, z format of 111, 107, 69 and 81, 68, 92, and a radius of 10 Å. Sampling was executed using a grid size of 1 Å. Prior to running Epock, the Ric-8 structures were aligned so that the placement of the sampling cylinder was equivalent, encompassing the α5-helix binding cavity. The resultant calculated cavities were visualized using ChimeraX (Figure S5).

Quantification and Statistical Analysis

Data from thermal shift assays were normalized to the fraction of maximal fluorescence and fit to a Boltzmann sigmoidal curve using GraphPad Prism (processing is derived from previously used methods for melt curve fitting[79] and normalization[80]). Data are presented as the best-fit curve from experiments performed in four biological replicates. The plotted ΔTm shift values of Ric-8A and Ric-8B at 150 μM peptide are represented as mean +/− S.D and statistical significance was calculated using repeated measures of one-way analysis of variance (ANOVA) using GraphPad Prism. Data from the cell-based Gαolf protein folding sensor assay are represented as mean +/− S.D. of at least three biologically-independent transfections, with a minimum of six technical replicates per condition. Data were normalized to the luminescent signal from WT Gαolf-RLuc with and without co-transfected WT Ric-8B, which was present on every plate read as a positive and negative control respectively. Statistical significance between chaperone binding was calculated using one-way ANOVA testing with GraphPad Prism. Protein relative abundance levels from Western Blot analyses were quantified in triplicate via pixel densitometry using Adobe Photoshop and represented as mean +/− S.D. prior to ANOVA comparison. All displayed P values from individual ANOVA tests are numerically described within their corresponding figure legend.

Supplementary Material

Refer to Web version on PubMed Central for supplementary material.

Acknowledgements

We thank the Stanford Cryo-Electron Microscopy Center (cEMc) for access to instrumentation and Alpay B. Seven for maintenance of computational resources. This work was funded by NIGMS RO1 088242 to G.G.T. The National Science Foundation Graduate Research Fellowship Program supported M.Y. under Grant No. DGE-1656518. Any opinions, findings, and conclusions or recommendations expressed in this material are those of the author(s) and do not necessarily reflect the views of the National Science Foundation.

References

1. Mixon MB, Lee E, Coleman DE, Berghuis AM, Gilman AG, and Sprang SR (1995). Tertiary and Quaternary Structural Changes in Giα1 Induced by GTP Hydrolysis. Science 270, 954–960. 10.1126/science.270.5238.95. [PubMed: 7481799]
2. Sunahara RK, Tesmer JJG, Gilman AG, and Sprang SR (1997). Crystal structure of the adenylyl cyclase activator G(s)alpha. Science 278, 1943–1947. 10.1126/science.278.5345.1943. [PubMed: 9395396]
3. Rasmussen SG, DeVree BT, Zou Y, Kruse AC, Chung KY, Kobilka TS, Thian FS, Chae PS, Pardon E, Calinski D, et al. (2011). Crystal structure of the beta2 adrenergic receptor-Gs protein complex. Nature 477, 549–555. 10.1038/nature10361. [PubMed: 21772288]
4. Lukov GL, Baker CM, Ludtke PJ, Hu T, Carter MD, Hackett RA, Thulin CD, and Willardson BM (2006). Mechanism of assembly of G protein betagamma subunits by protein kinase CK2-phosphorylated phosducin-like protein and the cytosolic chaperonin complex. J. Biol. Chem 281, 22261–22274. 10.1074/jbc.M601590200. [PubMed: 16717095]
5. Dupre DJ, Robitaille M, Richer M, Ethier N, Mamarbachi AM, and Hebert TE (2007). Dopamine receptor-interacting protein 78 acts as a molecular chaperone for Ggamma subunits before assembly with Gbeta. J. Biol. Chem 282, 13703–13715. 10.1074/jbc.M608846200. [PubMed: 17363375]

6. Lukov GL, Hu T, McLaughlin JN, Hamm HE, and Willardson BM (2005). Phosducin-like protein acts as a molecular chaperone for G protein betagamma dimer assembly. EMBO J 24, 1965–1975. 10.1038/sj.emboj.7600673. [PubMed: 15889144]
7. Plimpton RL, Cuellar J, Lai CW, Aoba T, Makaju A, Franklin S, Mathis AD, Prince JT, Carrascosa JL, Valpuesta JM, and Willardson BM (2015). Structures of the Gbeta-CCT and PhLP1-Gbeta-CCT complexes reveal a mechanism for G-protein beta-subunit folding and Gbetagamma dimer assembly. Proc. Natl. Acad. Sci. USA 112, 2413–2418. 10.1073/pnas.1419595112. [PubMed: 25675501]
8. Evanko DS, Thiyagarajan MM, and Wedegaertner PB (2000). Interaction with Gbetagamma is required for membrane targeting and palmitoylation of Galpha(s) and Galpha(q). J. Biol. Chem 275, 1327–1336. 10.1074/jbc.275.2.1327. [PubMed: 10625681]
9. Chan P, Gabay M, Wright FA, and Tall GG (2011). Ric-8B is a GTP-dependent G protein alphas guanine nucleotide exchange factor. J. Biol. Chem 286, 19932–19942. 10.1074/jbc.M110.163675. [PubMed: 21467038]
10. Miller KG, Emerson MD, McManus JR, and Rand JB (2000). RIC-8 (Synembryn): A Novel Conserved Protein that Is Required for G(q)alpha Signaling in the C. elegans Nervous System. Neuron 27, 289–299. 10.1016/s0896-6273(00)00037-4. [PubMed: 10985349]
11. Tall GG, Krumins AM, and Gilman AG (2003). Mammalian Ric-8A (synembryn) is a heterotrimeric Galpha protein guanine nucleotide exchange factor. J. Biol. Chem 278, 8356–8362. 10.1074/jbc.M211862200. [PubMed: 12509430]
12. Gabay M, Pinter ME, Wright FA, Chan P, Murphy AJ, Valenzuela DM, Yancopoulos GD, and Tall GG (2011). Ric-8 Proteins Are Molecular Chaperones That Direct Nascent G Protein a Subunit Membrane Association. Sci. Signal 4. 10.1126/scisignal.2002223.
13. Woodard GE, Huang NN, Cho H, Miki T, Tall GG, and Kehrl JH (2010). Ric-8A and Gi alpha recruit LGN, NuMA, and dynein to the cell cortex to help orient the mitotic spindle. Mol. Cell. Biol 30, 3519–3530. 10.1128/MCB.00394-10. [PubMed: 20479129]
14. Wang L, Guo D, Xing B, Zhang JJ, Shu HB, Guo L, and Huang XY (2011). Resistance to inhibitors of cholinesterase-8A (Ric-8A) is critical for growth factor receptor-induced actin cytoskeletal reorganization. J. Biol. Chem 286, 31055–31061. 10.1074/jbc.M111.253427. [PubMed: 21771786]
15. Nagai Y, Nishimura A, Tago K, Mizuno N, and Itoh H (2010). Ric-8B stabilizes the alpha subunit of stimulatory G protein by inhibiting its ubiquitination. J. Biol. Chem 285, 11114–11120. 10.1074/jbc.M109.063313. [PubMed: 20133939]
16. Miller KG, and Rand JB (2000). A role for RIC-8 (Synembryn) and GOA-1 (G(o)alpha) in regulating a subset of centrosome movements during early embryogenesis in C*aenorhabditis elegans*. Genetics 156, 1649–1660. 10.1093/genetics/156.4.1649. [PubMed: 11102364]
17. Nishimura A, Okamoto M, Sugawara Y, Mizuno N, Yamauchi J, and Itoh H (2006). Ric-8A potentiates Gq-mediated signal transduction by acting downstream of G protein-coupled receptor in intact cells. Genes Cells 11, 487–498. 10.1111/j.1365-2443.2006.00959.x. [PubMed: 16629901]
18. Reynolds NK, Schade MA, and Miller KG (2005). Convergent, RIC-8-dependent Galpha signaling pathways in the Caenorhabditis elegans synaptic signaling network. Genetics 169, 651–670. 10.1534/genetics.104.031286. [PubMed: 15489511]
19. Afshar K, Willard FS, Colombo K, Johnston CA, McCudden CR, Siderovski DP, and Gonczy P (2004). RIC-8 is required for GPR-1/2-dependent Galpha function during asymmetric division of C. elegans embryos. Cell 119, 219–230. 10.1016/j.cell.2004.09.026. [PubMed: 15479639]
20. David NB, Martin CA, Segalen M, Rosenfeld F, Schweisguth F, and Bellaiche Y (2005). Drosophila Ric-8 regulates Galphai cortical localization to promote Galphai-dependent planar orientation of the mitotic spindle during asymmetric cell division. Nat. Cell Biol 7, 1083–1090. 10.1038/ncb1319. [PubMed: 16228010]
21. Hampoelz B, Hoeller O, Bowman SK, Dunican D, and Knoblich JA (2005). Drosophila Ric-8 is essential for plasma-membrane localization of heterotrimeric G proteins. Nat. Cell Biol 7, 1099–1105. 10.1038/ncb1318. [PubMed: 16228011]

22. Chan P, Thomas CJ, Sprang SR, and Tall GG (2013). Molecular chaperoning function of Ric-8 is to fold nascent heterotrimeric G protein alpha subunits. Proc. Natl. Acad. Sci. USA 110, 3794–3799. 10.1073/pnas.1220943110. [PubMed: 23431197]
23. Papasergi MM, Patel BR, and Tall GG (2015). The G protein alpha chaperone Ric-8 as a potential therapeutic target. Mol. Pharmacol 87, 52–63. 10.1124/mol.114.094664. [PubMed: 25319541]
24. Wilkie TM, and Kinch L (2005). New roles for Galpha and RGS proteins: communication continues despite pulling sisters apart. Curr. Biol 15, R843–854. 10.1016/j.cub.2005.10.008. [PubMed: 16243026]
25. Von Dannecker LE, Mercadante AF, and Malnic B (2006). Ric-8B promotes functional expression of odorant receptors. Proc. Natl. Acad. Sci. USA 103, 9310–9314. 10.1073/pnas.0600697103. [PubMed: 16754875]
26. Von Dannecker LE, Mercadante AF, and Malnic B (2005). Ric-8B, an Olfactory Putative GTP Exchange Factor, Amplifies Signal Transduction through the Olfactory-Specific G-Protein G olf. J. Neurosci 25, 3793–3800. 10.1523/jneurosci.4595-04.2005. [PubMed: 15829631]
27. Kerr DS, Von Dannecker LE, Davalos M, Michaloski JS, and Malnic B (2008). Ric-8B interacts with G alpha olf and G gamma 13 and co-localizes with G alpha olf, G beta 1 and G gamma 13 in the cilia of olfactory sensory neurons. Mol. Cell. Neurosci 38, 341–348. 10.1016/j.mcn.2008.03.006. [PubMed: 18462949]
28. Chan P, Gabay M, Wright FA, Kan W, Oner SS, Lanier SM, Smrcka AV, Blumer JB, and Tall GG (2011). Purification of heterotrimeric G protein alpha subunits by GST-Ric-8 association: primary characterization of purified G alpha(olf). J. Biol. Chem 286, 2625–2635. 10.1074/jbc.M110.178897. [PubMed: 21115479]
29. Machado CF, Nagai MH, Lyra CS, Reis-Silva TM, Xavier AM, Glezer I, Felicio LF, and Malnic B (2017). Conditional Deletion of Ric-8b in Olfactory Sensory Neurons Leads to Olfactory Impairment. J. Neurosci 37, 12202–12213. 10.1523/JNEUROSCI.0943-17.2017. [PubMed: 29118104]
30. Zeng B, Mou TC, Doukov TI, Steiner A, Yu W, Papasergi-Scott M, Tall GG, Hagn F, and Sprang SR (2019). Structure, Function, and Dynamics of the Galpha Binding Domain of Ric-8A. Structure 27, 1137–1147 e1135. 10.1016/j.str.2019.04.013. [PubMed: 31155309]
31. Srivastava D, Gakhar L, and Artemyev NO (2019). Structural underpinnings of Ric8A function as a G-protein alpha-subunit chaperone and guanine-nucleotide exchange factor. Nat. Commun 10, 3084. 10.1038/s41467-019-11088-x. [PubMed: 31300652]
32. McClelland LJ, Zhang K, Mou TC, Johnston J, Yates-Hansen C, Li S, Thomas CJ, Doukov TI, Triest S, Wohlkonig A, et al. (2020). Structure of the G protein chaperone and guanine nucleotide exchange factor Ric-8A bound to Galphai1. Nat. Commun 11, 1077. 10.1038/s41467-020-14943-4. [PubMed: 32103024]
33. Seven AB, Hilger D, Papasergi-Scott MM, Zhang L, Qu Q, Kobilka BK, Tall GG, and Skiniotis G (2020). Structures of Galpha Proteins in Complex with Their Chaperone Reveal Quality Control Mechanisms. Cell Rep 30, 3699–3709 e3696. 10.1016/j.celrep.2020.02.086. [PubMed: 32126208]
34. Papasergi-Scott MM, Stoveken HM, MacConnachie L, Chan P-Y, Gabay M, Wong D, Freeman RS, Beg AA, and Tall GG (2018). Dual phosphorylation of Ric-8A enhances its ability to mediate G protein a subunit folding and to stimulate guanine nucleotide exchange. Sci. Signal 11, eaap8113. 10.1126/scisignal.aap8113. [PubMed: 29844055]
35. Yu W, Yu M, Papasergi-Scott MM, and Tall GG (2019). Production of Phosphorylated Ric-8A proteins using protein kinase CK2. Protein Expr. Purif 154, 98–103. 10.1016/j.pep.2018.10.002. [PubMed: 30290220]
36. Thomas CJ, Briknarova K, Hilmer JK, Movahed N, Bothner B, Sumida JP, Tall GG, and Sprang SR (2011). The nucleotide exchange factor Ric-8A is a chaperone for the conformationally dynamic nucleotide-free state of Gαi1. PLoS One 6, e23197. 10.1371/journal.pone.0023197. [PubMed: 21853086]
37. Yano H, Provasi D, Cai NS, Filizola M, Ferre S, and Javitch JA (2017). Development of novel biosensors to study receptor-mediated activation of the G-protein alpha subunits Gs and Golf. J. Biol. Chem 292, 19989–19998. 10.1074/jbc.M117.800698. [PubMed: 29042444]

38. Kant R, Zeng B, Thomas CJ, Bothner B, and Sprang SR (2016). Ric-8A, a G protein chaperone with nucleotide exchange activity induces long-range secondary structure changes in Galpha. Elife 5. 10.7554/eLife.19238.
39. Conklin BR, Farfelt Z, Lustig KD, Julius D, and Bourne HR (1993). Substitution of three amino acids switches receptor specificity of Gqα to that of Giα. Nature 363, 274–276. 10.1038/363274a0. [PubMed: 8387644]
40. Oldham WM, and Hamm HE (2008). Heterotrimeric G protein activation by G-protein-coupled receptors. Nat. Rev. Mol. Cell Biol 9, 60–71. 10.1038/nrm2299. [PubMed: 18043707]
41. Kaya AI, Lokits AD, Gilbert JA, Iverson TM, Meiler J, and Hamm HE (2016). A Conserved Hydrophobic Core in Galphai1 Regulates G Protein Activation and Release from Activated Receptor. J. Biol. Chem 291, 19674–19686. 10.1074/jbc.M116.745513. [PubMed: 27462082]
42. Jang W, Lu S, Xu X, Wu G, and Lambert NA (2023). The role of G protein conformation in receptor-G protein selectivity. Nat. Chem. Biol 20230116. 10.1038/s41589-022-01231-z.
43. Jumper J, Evans R, Pritzel A, Green T, Figurnov M, Ronneberger O, Tunyasuvunakool K, Bates R, Zidek A, Potapenko A, et al. (2021). Highly accurate protein structure prediction with AlphaFold. Nature 596, 583–589. 10.1038/s41586-021-03819-2. [PubMed: 34265844]
44. Oner SS, Maher EM, Gabay M, Tall GG, Blumer JB, and Lanier SM (2013). Regulation of the G-protein regulatory-Galphai signaling complex by nonreceptor guanine nucleotide exchange factors. J. Biol. Chem 288, 3003–3015. 10.1074/jbc.M112.418467. [PubMed: 23212907]
45. Punjani A, and Fleet DJ (2021). 3D variability analysis: Resolving continuous flexibility and discrete heterogeneity from single particle cryo-EM. J. Struct. Biol 213, 107702. 10.1016/j.jsb.2021.107702. [PubMed: 33582281]
46. Osawa S, Dhanasekaran N, Woon CW, and Johnson GL (1990). Gαi-Gαs Chimeras Define the Funciton of α Chain Domains in Control of G Protein Activation and ßg Subunit Complex Interactions. Cell 63, 697–706. 10.1016/0092-8674(90)90136-3. [PubMed: 2121366]
47. Itoh H, and Gilman AG (1991). Expression and Analysis of Gsα Mutants with Decreased Ability to Activate Adenylylcyclase. J. Biol. Chem 266, 16226–16231. 10.1016/S0021-9258(18)98539-X. [PubMed: 1651937]
48. Berlot CH, and Bourne H (1992). Identification of Effector-Activating Residues of Gsα. Cell 68, 911–922. 10.1016/0092-8674(92)90034-A. [PubMed: 1547491]
49. Qiao A, Han S, Li X, Li Z, Zhao P, Dai A, Chang R, Tai L, Tan Q, Chu X, et al. (2020). Structural basis of Gs and Gi recognition by the human glucagon receptor. Science 367, 1346–1352. 10.1126/science.aaz5346. [PubMed: 32193322]
50. Rose AS, Elgeti M, Zachariae U, Grubmuller H, Hofmann KP, Scheerer P, and Hildebrand PW (2014). Position of transmembrane helix 6 determines receptor G protein coupling specificity. J. Am. Chem. Soc 136, 11244–11247. 10.1021/ja5055109. [PubMed: 25046433]
51. Kang Y, Kuybeda O, de Waal PW, Mukherjee S, Van Eps N, Dutka P, Zhou XE, Bartesaghi A, Erramilli S, Morizumi T, et al. (2018). Cryo-EM structure of human rhodopsin bound to an inhibitory G protein. Nature 558, 553–558. 10.1038/s41586-018-0215-y. [PubMed: 29899450]
52. Maeda S, Qu Q, Robertson MJ, Skiniotis G, and Kobilka BK (2019). Structures of the M1 and M2 muscarinic acetylcholine receptor/G-protein complexes. Science 364, 552–557. 10.1126/science.aaw5188. [PubMed: 31073061]
53. O'Hayre M, Vazquez-Prado J, Kufareva I, Stawiski EW, Handel TM, Seshagiri S, and Gutkind JS (2013). The emerging mutational landscape of G proteins and G-protein-coupled receptors in cancer. Nat. Rev. Cancer 13, 412–424. 10.1038/nrc3521. [PubMed: 23640210]
54. Wheeler EC, Vora S, Mayer D, Kotini AG, Olszewska M, Park SS, Guccione E, Teruya-Feldstein J, Silverman L, Sunahara RK, et al. (2021). Integrative RNA-omics discovers GNAS alternative splicing as a phenotypic driver of splicing factor-mutant neoplasms. Cancer Discov 2021/10/09. 10.1158/2159-8290.CD-21-0508.
55. Zhu X, Boman AL, Kuai J, Cieplak W, and Kahn RA (2000). Effectors increase the affinity of ADP-ribosylation factor for GTP to increase binding. J. Biol. Chem 275, 13465–13475. 10.1074/jbc.275.18.13465. [PubMed: 10788460]

56. Linder ME, Middleton P, Hepler JR, Taussig R, Gilman AG, and Mumby SM (1993). Lipid modification of G proteins: alpha subunits are palmitoylated. Proc. Natl. Acad. Sci. USA 90, 3675–3679. 10.1073/pnas.90.8.3675. [PubMed: 8475115]
57. Vizcaino JA, Deutsch EW, Wang R, Csordas A, Reisinger F, Rios D, Dianes JA, Sun Z, Farrah T, Bandeira N, et al. (2014). ProteomeXchange provides globally coordinated proteomics data submission and dissemination. Nat. Biotechnol 32, 223–226. 10.1038/nbt.2839. [PubMed: 24727771]
58. English JG, Shellhammer JP, Malahe M, McCarter PC, Elston TC, and Dohlman HG (2015). MAPK feedback encodes a switch and timer for tunable stress adaptation in yeast. Sci. Signal 8, ra5. 10.1126/scisignal.2005774. [PubMed: 25587192]
59. Kapust RB, Tózsér J, Fox JD, Anderson DE, Cherry S, Copeland TD, and Waugh DS (2001). Tobacco etch virus protease: mechanism of autolysis and rational design of stable mutants with wild-type catalytic proficiency. Protein Eng 14, 993–1000. 10.1093/protein/14.12.993. [PubMed: 11809930]
60. Ran FA, Hsu PD, Wright J, Agarwala V, Scott DA, and Zhang F (2013). Genome engineering using the CRISPR-Cas9 system. Nat. Protoc 8, 2281–2308. 10.1038/nprot.2013.143. [PubMed: 24157548]
61. Ryan JA (2008). Cell cloning by serial dilution in 96 well plates protocol Corning Inc.
62. Dyer BW, Ferrer FA, Klinedinst DK, and Rodriguez R (2000). A noncommercial dual luciferase enzyme assay system for reporter gene analysis. Anal. Biochem 282, 158–161. 10.1006/abio.2000.4605. [PubMed: 10860516]
63. Brenner S, and Horne RW (1959). A negative staining method for high resolution electron microscopy of viruses. Biochimica et Biophysica Acta 34, 103–110. 10.1016/0006-3002(59)90237-9. [PubMed: 13804200]
64. Peisley A, and Skiniotis G (2015). 2D Projection Analysis of GPCR Complexes by Negative Stain Electron Microscopy. Methods Mol. Biol 1335, 29–38. 10.1007/978-1-4939-2914-6_3. [PubMed: 26260592]
65. Mastronarde DN (2005). Automated electron microscope tomography using robust prediction of specimen movements. J. Struct. Biol 152, 36–51. 10.1016/j.jsb.2005.07.007. [PubMed: 16182563]
66. Zheng SQ, Palovcak E, Armache JP, Verba KA, Cheng Y, and Agard DA (2017). MotionCor2: anisotropic correction of beam-induced motion for improved cryo-electron microscopy. Nat. Methods 14, 331–332. 10.1038/nmeth.4193. [PubMed: 28250466]
67. Rohou A, and Grigorieff N (2015). CTFFIND4: Fast and accurate defocus estimation from electron micrographs. J. Struct. Biol 192, 216–221. 10.1016/j.jsb.2015.08.008. [PubMed: 26278980]
68. Scheres SH (2016). Processing of Structurally Heterogeneous Cryo-EM Data in RELION. Methods Enzymol 579, 125–157. 10.1016/bs.mie.2016.04.012. [PubMed: 27572726]
69. Punjani A, Rubinstein JL, Fleet DJ, and Brubaker MA (2017). cryoSPARC: algorithms for rapid unsupervised cryo-EM structure determination. Nat. Methods 14, 290–296. 10.1038/nmeth.4169. [PubMed: 28165473]
70. Punjani A, Zhang H, and Fleet DJ (2020). Non-uniform refinement: adaptive regularization improves single-particle cryo-EM reconstruction. Nat. Methods 17, 1214–1221. 10.1038/s41592-020-00990-8. [PubMed: 33257830]
71. Pettersen EF, Goddard TD, Huang CC, Couch GS, Greenblatt DM, Meng EC, and Ferrin TE (2004). UCSF Chimera--a visualization system for exploratory research and analysis. J. Comput. Chem 25, 1605–1612. 10.1002/jcc.20084. [PubMed: 15264254]
72. Pettersen EF, Goddard TD, Huang CC, Meng EC, Couch GS, Croll TI, Morris JH, and Ferrin TE (2021). UCSF ChimeraX: Structure visualization for researchers, educators, and developers. Protein Sci 30, 70–82. 10.1002/pro.3943. [PubMed: 32881101]
73. Bayly-Jones C (2022). Wiggle (GitHub).
74. Waterhouse A, Bertoni M, Bienert S, Studer G, Tauriello G, Gumienny R, Heer FT, de Beer TAP, Rempfer C, Bordoli L, et al. (2018). SWISS-MODEL: homology modelling of protein structures and complexes. Nucleic Acids Res. 46, W296–W303. 10.1093/nar/gky427. [PubMed: 29788355]
75. Emsley P, Lohkamp B, Scott WG, and Cowtan K (2010). Features and development of Coot. Acta Crystallogr. D Struct. Biol 66, 486–501. 10.1107/S0907444910007493.

76. Liebschner D, Afonine PV, Baker ML, Bunkoczi G, Chen VB, Croll TI, Hintze B, Hung LW, Jain S, McCoy AJ, et al. (2019). Macromolecular structure determination using X-rays, neutrons and electrons: recent developments in Phenix. Acta Crystallogr. D Struct. Biol 75, 861–877. 10.1107/S2059798319011471.

77. Humphrey W, Dalke A, and Schulten K (1996). VMD: Visual Molecular Dynamics. J. Mol. Graph 14, 33–38. 10.1016/0263-7855(96)00018-5. [PubMed: 8744570]

78. Laurent B, Chavent M, Cragnolini T, Dahl AC, Pasquali S, Derreumaux P, Sansom MS, and Baaden M (2015). Epock: rapid analysis of protein pocket dynamics. Bioinformatics 31, 1478–1480. 10.1093/bioinformatics/btu822. [PubMed: 25505095]

79. Huynh K, and Partch CL (2015). Analysis of protein stability and ligand interactions by thermal shift assay. Curr. Protoc. Protein Sci 79, 28 29 21–28 29 14. 10.1002/0471140864.ps2809s79.

80. Sun C, Li Y, Yates EA, and Fernig DG (2020). SimpleDSFviewer: A tool to analyze and view differential scanning fluorimetry data for characterizing protein thermal stability and interactions. Protein Sci 29, 19–27. 10.1002/pro.3703. [PubMed: 31394001]

Highlights:

- Structures of Ric-8B in complex with its folding clients Gαolf and Gαs
- Ric-8B has a more permissive Gα subunit α5 helix binding pocket than Ric-8A
- Ric-8B accommodates the unique i3 loop of Gαs/olf.
- A new *RIC-8B*-deletion cell line with Gαolf folding sensor was created.

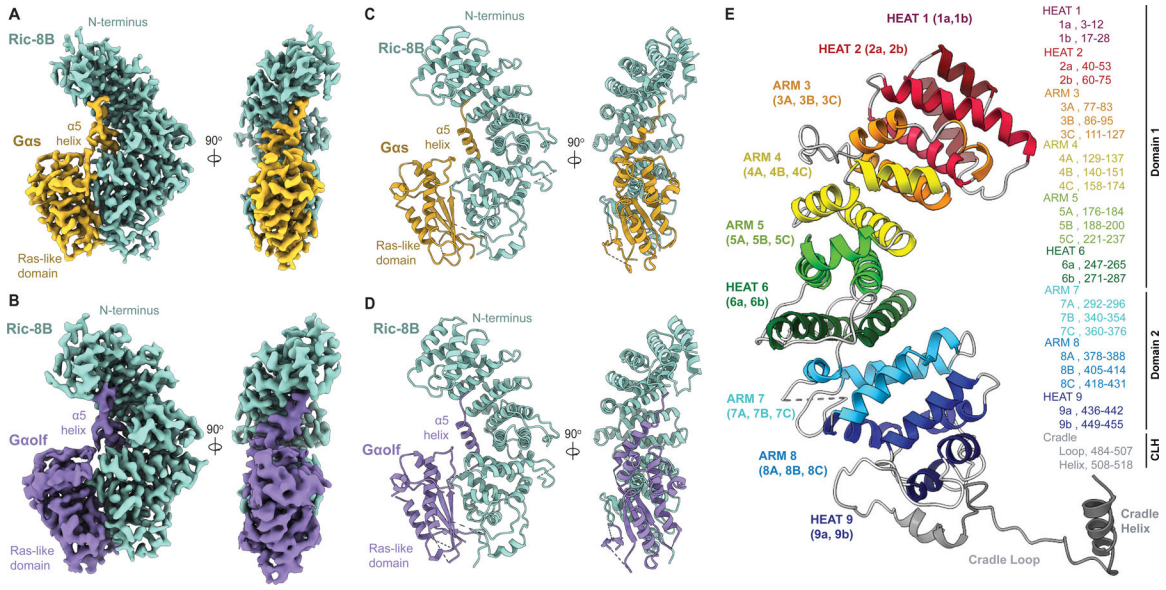

Figure 1.

CryoEM reconstructions of Ric-8B in complex with Gαs and Gαolf. (A, B) CryoEM maps and (C, D) ribbon diagrams of Ric-8B (teal) with Gαs (gold, A and C) or Gαolf (purple, B and D). (E) Ric-8B structure shown by ribbon diagram and definition of elements. Individual α-helices are named by helical repeat number, from N-terminus to C-terminus, and by position within repeat. HEAT repeats consist of two α-helices and are lettered lowercase ‘a’ and ‘b’, while ARM repeats contain three α-helices lettered uppercase ‘A’, ‘B’, and ‘C’. See also Figure S1 and S2, and Table S2.

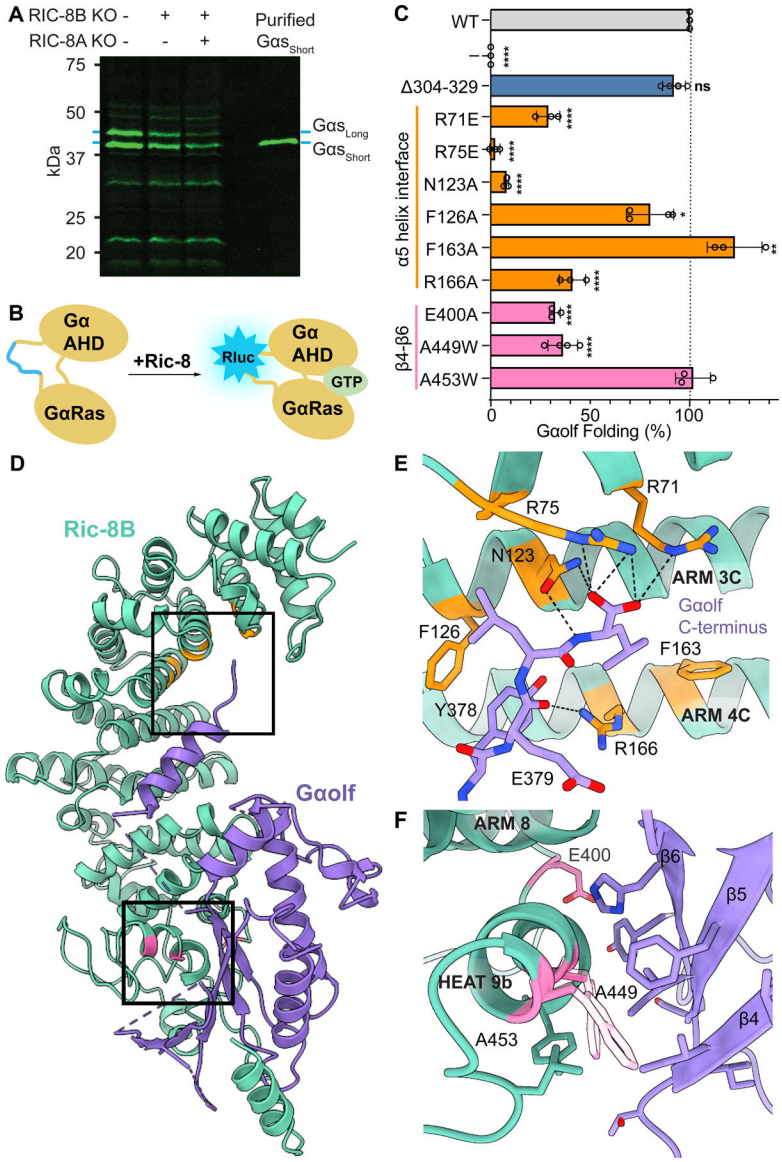

Figure 2.

Structure-guided mutational analysis of Ric-8B folding activity. (A) Validation of *RIC-8B* gene deletion by immunoblot quantification of Gαs protein abundance in wild type, *RIC-8B*$^{-/-}$ *or RIC-8A*$^{-/-}$;*RIC-8B*$^{-/-}$ double knockout HEK293T cells. In *RIC-8B* knockout cells, the Gαolf sensor produced a dim luminescence signal that was enhanced markedly by transfection of wild type Ric-8B. (B) Cartoon representation of the Gαolf protein folding sensor with an internal *Renilla* luciferase (RLuc) module. (C) The effects on Gαolf sensor folding upon mutagenesis of key Ric-8B residues deduced from the structures to be important interaction sites between Ric-8B and Gαs/olf. (D-F) Global and focused ribbon diagram views depicting Ric-8B interaction sites with the Gαs/olf (E) α5-helix interface and (F) β4-β6 sheet region. Data represent the mean of experiments performed in at least triplicate with error bars representing +/− S.D. * = $p < 0.05$, ** = $p < 0.01$, *** = $p < 0.001$, **** = $p < 0.0001$. See also Figure S3 and S4.

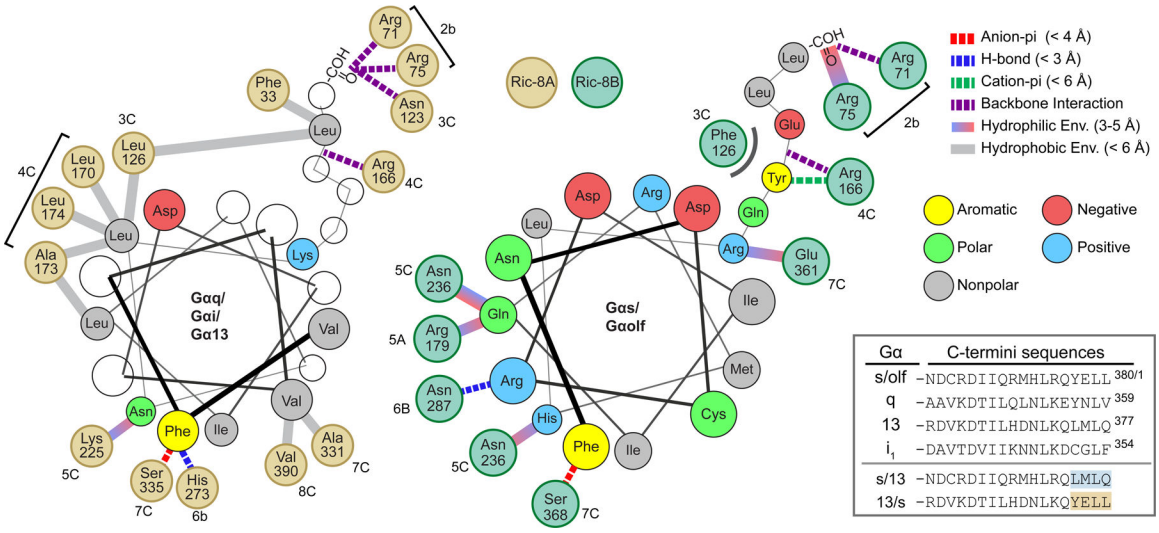

Figure 3.

Ric-8B interactions with the Gα α5 helix are generally hydrophilic and polar in nature, while Ric-8A interactions with the Gα α5 helix are primarily hydrophobic. Interaction between Ric-8 proteins with the Gα α5 helices represented with helical-wheel diagrams. Non-helical C-terminal residues continue to the upper right of each diagram. Specific interactions of Gα residues with Ric-8 α-helical repeat elements are noted in bold black lettering (*e.g.,* 2b, etc.).

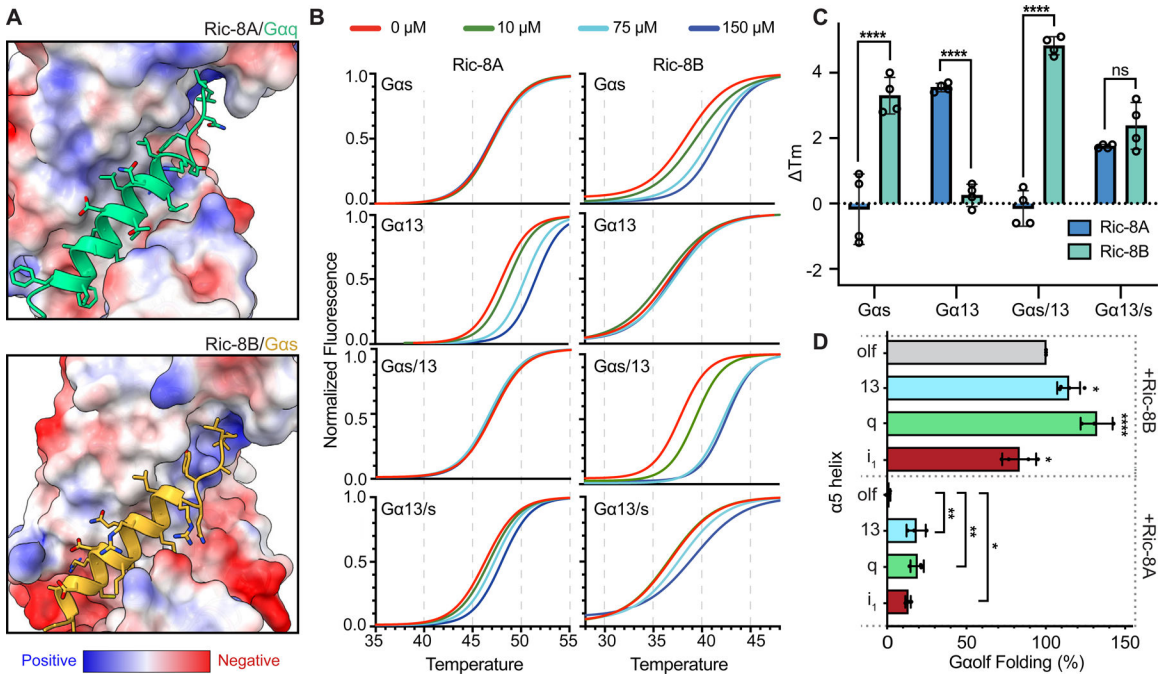

Figure 4.

Contribution of the Gα C-terminus and α5 helix to Ric-8 isoform specificity. (A) Electrostatic surface maps of the Gα α5 helix binding pockets of Ric-8A in complex with Gαq (top) and Ric-8B in complex with Gαs (bottom). (B) Ric-8A and Ric-8B protein thermal stability assays with synthetic peptides comprising the last 18 residues of Gαs and Gα13 or chimeric Gα peptides with swaps of the last four residues (*e.g.,* Gαs/13 is 14 residues Gαs / 4 residues Gα13). (C) Quantification of maximal ΔTm shifts for (B) Ric-8A (blue) and Ric-8B (green). (D) Ric-8A- and Ric-8B-dependent cell-based folding assay of chimeric Gαolf sensors consisting of 18 C-terminal Gα residue swaps for Gα13, Gαq, $G\alpha i_1$. Ric-8B indiscriminately folded each sensor. A partial gain of folding function was observed for Ric-8A only when C-termini of its Gα substrates were swapped into the Gαolf sensor. Data represent the mean of experiments performed in at least triplicate with error bars representing +/− S.D. * = $p < 0.05$, ** = $p < 0.01$, *** = $p < 0.001$, **** = $p < 0.0001$. See also Figure S5 and S6.

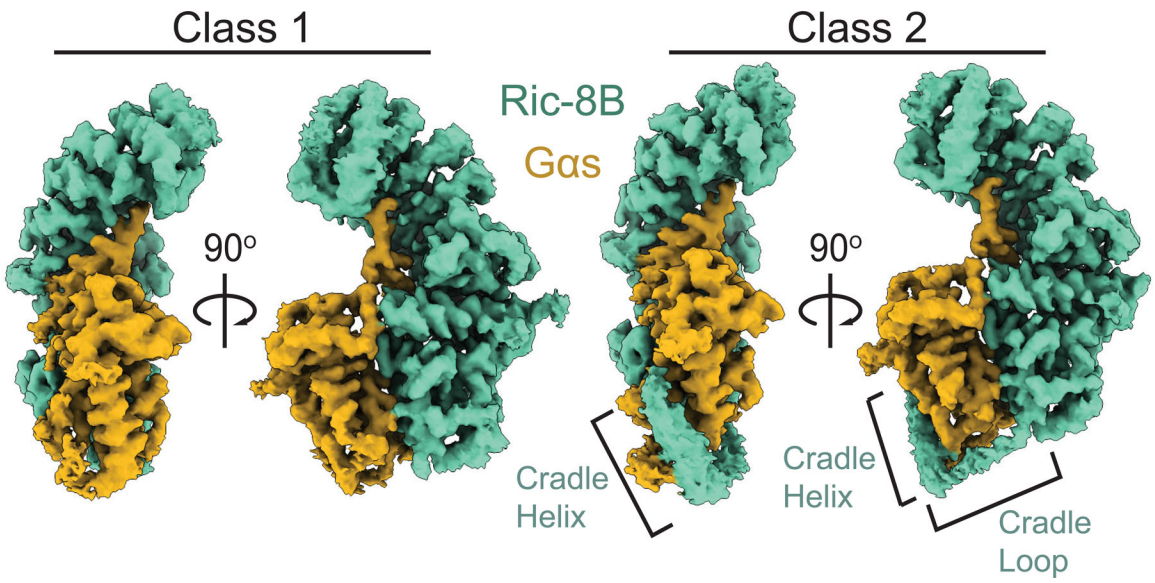

Figure 5.

3D variability analysis summary of the Ric-8B/Gαs complex. Two representations of discrete particle subsets within the cryoEM dataset reveal heterogeneity within the Ric-8B/Gαs complex. Notably, the cradle loop helix (CLH) is conformationally heterogeneous across classes. See also Figure S7.

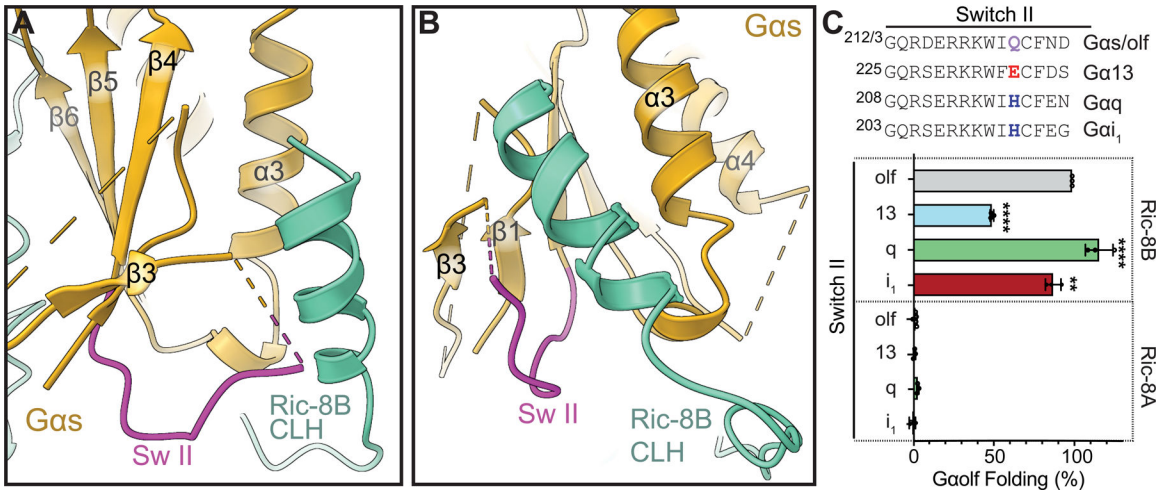

Figure 6.

Analysis of Gα Switch II interactions with Ric-8. (A-B) Detailed views of the region containing Gαs Switch II (pink) engaged by Ric-8B (PDB ID: 8EL7). The Ric-8B CLH interacts with the Gαs α3 helix and Switch II. (C) Ric-8B and Ric-8A folding of the Gαolf sensor (grey) compared to folding of Gα13, Gαq- and $Gαi_1$ Switch II / Gαolf chimeric sensors. Switch II sequence alignments of Gα subunits tested. Gαs/olf Q222 (purple) has polarity difference compared to equivalent residues of the other Gα subunits (E, red and H, blue). Data represent the mean of experiments performed in at least triplicate with error bars representing +/− S.D. * = $p < 0.05$, ** = $p < 0.01$, *** = $p < 0.001$, **** = $p < 0.0001$. See also Figure S6.

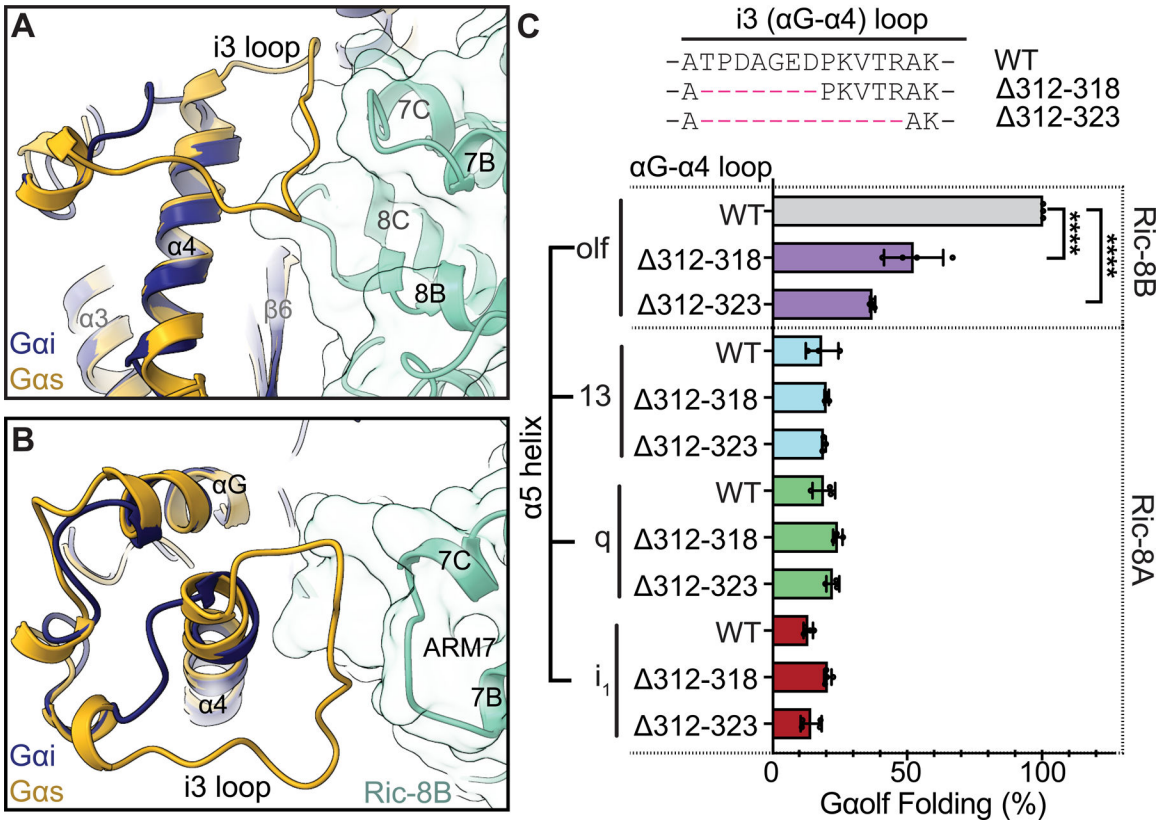

Figure 7.

Analysis of Gα αG-α4 (i3) loop interactions with Ric-8 and the dependence for Gα subunit folding. (A-B) Zoomed in views of overlaid αG-α4 connecting loops from the Gαs / Ric-8B complex (gold, PDB ID: 8EL7) and the $G\alpha i_1$ / Ric-8A complex (violet, PDB ID: 6VU8) showing the positioning of the extra i3 loop insertion within Gαs and its contacts with the ARM 7B-7C loop of Ric-8B (teal). (C) Sequence alignment of the Gαolf αG-α4 (i3) loop and two engineered i3 deletions (Δ312–318 or Δ312–323) that were tested in the Gαolf sensor folding assay. Ablation of the extra Gαolf i3 insertion had substantial impact on Ric-8B-mediated folding but had no impact on Ric-8A-mediated folding even in the context of swaps of the Gαolf α5 helix for Gα13, Gαq or $G\alpha i_1$ α5 helices. Data represent the mean of experiments performed in at least triplicate with error bars representing +/− S.D. * = $p < 0.05$, ** = $p < 0.01$, *** = $p < 0.001$, **** = $p < 0.0001$. See also Figure S6.

KEY RESOURCES TABLE

REAGENT or RESOURCE	SOURCE	IDENTIFIER
Antibodies		
Rabbit polyclonal antiserum 2413 against Ric-8B	Chan et al., 2013; Gabay et al., 2011	N/A
Rabbit polyclonal antiserum 1184 against Ric-8A	Chan et al., 2013; Gabay et al., 2011	N/A
G protein subunit antiserum B600 against Gβ1–4	Linder et al., 1993	N/A
IgG purified polyclonal antibodies for Gαs	Millipore Sigma	Cat#06–237
IgG purified polyclonal antibodies for Gαq/11	Millipore Sigma	Cat#06–709
IgG purified monoclonal antibody for GAPDH	Invitrogen	ZG003
Phospho-CK2 Substrate [(pS/pT)DXE] MultiMab™ Rabbit mAb mix	Cell Signaling Technology	#8738
Enriched IgG fraction of rabbit antiserum against Ric-8B pSer468/Ric-8A pSer435	Papasergi-Scott et al., 2018	N/A
Bacterial and Virus Strains		
E. coli Rosetta 2 (DE3)pLysS	Novagen	Cat#71397
E. coli DH10 Bac	Invitrogen	Cat#10361012
E. coli DH5a	Invitrogen	Cat#18258012
Chemicals, Peptides, and Recombinant Proteins		
Phos-tag Acrylamide	Wako Chemical Industries	Product Number AAL-107
Protein Kinase CK2 holoenzyme	New England Biolabs	P6010
Phenylmethylsulfonyl fluoride	Sigma	Cat#P7626
Na-p-tosyl-L-lysine-chloromethyl ketone	Sigma	Cat#T7254
L-1-p-tosylamino-2-phenylethyl-chloromethyl ketone	Sigma	Cat#T4376
leupeptin (hemisulfate)	Cayman Chemical	Cat#14026
trypsin inhibitor from lima bean	Sigma	Cat#T9378
Dithiothreitol	Sigma	Cat#D9779
NP-40	Thermo Scientific	Cat#28324
ATP disodium salt	Sigma	Cat#A3377
CHAPS	G-Biosciences	Cat#DG051
NaF	JT Baker	Cat#3688–01
$AlCl_3$	Fisher	Cat#A573
GDP sodium salt	Sigma	Cat#G7127
iodoacetamide	Promega	Cat#VB1010
trypsin	Promega	Cat#V5111
chymotrypsin	Promega	Cat#V1061
formic acid	Sigma	Cat#F0507
Gαs C-term amidated peptide: NDCRDIIQRMHLRQYELL	Genscript	N/A
Gα13 C-term amidated peptide: RDVKDTILHDNLKQLMLQ	Genscript	N/A

REAGENT or RESOURCE	SOURCE	IDENTIFIER
Gαs/Gα13 C-term chimera amidated peptide: NDCRDIIQRMHLRQLMLQ	Genscript	N/A
Gα13/Gαs C-term chimera amidated peptide: RDVKDTILHDNLKQYELL	Genscript	N/A
Sypro Orange	Sigma	Cat. #S5692
cyclohexamide	Sigma	Cat#01810
coelenterazine H	NanoLight Technology	Cat#301–5
M-PER	Thermo Scientific	Cat#78501
Triton-X 100	Bio-Rad	Cat#161–0407
Lipofectamine 2000	Invitrogen	Cat#11668–027
Critical Commercial Assays		
TaqMan Gene Expression assay	Applied Biosystems	Cat#4331182
Deposited Data		
Cryo-EM structure of Ric-8B/Gαs	This paper	EMDB-28223; PDB-8EL7
Cryo-EM structure of Ric-8B/Gαolf	This paper	EMDB-28224; PDB-8EL8
Cryo-EM structure of Ric-8A/Gαi1	Seven et al., 2020	PDB-6VU8
Cryo-EM structure of Ric-8A/Gαq	Seven et al., 2020	PDB-6VU5
AlphaFold predicted structure of *D. melanogaster* Ric-8	Jumper et al., 2021	AF-Q9GSX9-F1
Alpha Fold predicted structure of *C. elegans* Ric-8	Jumper et al., 2021	AF-Q9W358-F1
Mass spectrometry proteomics for Ric-8B	This paper	PXD036645
Experimental Models: Cell Lines		
HEK293T: *RIC-8B* knockout	This paper	N/A
HEK293T: *RIC-8B, RIC-8A* knockout	This paper	N/A
HEK293T: *RIC-8A* knockout	Papasergi-Scott et al., 2018	N/A
HEK293T	ATCC	CRL-11268
High Five cells: *Trichuplusia ni*	Expression Systems	Cat# 94–002S
Oligonucleotides		
RIC-8B guide RNA: 5'-TGTGACGGTAGACAGTTGGA-3'	IDT	N/A
Primers used in this study are listed in Supplementary Table 3	This paper	N/A
Recombinant DNA		
pcDNA 3.1 mouse Ric-8B	Gabay et al., 2011	N/A
pFastBac1 GST-TEV- mouse Ric-8B	Tall et al., 2003	N/A
pcDNA 3.1/hygromycin rat Ric-8A	Seven et al., 2020	N/A
pET21a GST-TEV mouse Ric-8B	Chan et al., 2011b	N/A
pcDNA 3.1 *Ce* Ric-8	This paper	N/A
pcDNA 3.1 *Dm* Ric-8	This paper	N/A
pcDNA 3.1 Gαolf-Rluc	Yano et al., 2017	N/A
pcDNA 3.1 Gαolf-mVenus	Yano et al., 2017	N/A
pcDNA 3.1 mouse Ric-8B point mutation plasmids listed in Supplementary Table 4	This paper	N/A

REAGENT or RESOURCE	SOURCE	IDENTIFIER
pcDNA 3.1 Gαolf-Rluc chimeric mutation plasmids listed in Supplementary Table 4	This paper	N/A
Software and Algorithms		
Prism 9	GraphPad software	https://www.graphpad.com/
Photoshop	Adobe	https://www.adobe.com/
Mascot	Matrix Science	https://www.matrixscience.com/
Scaffold	Proteome Software	https://www.proteomesoftware.com/products/scaffold-5
SerialEM	Mastronarde, 2005	https://bio3d.colorado.edu/SerialEM/
MotionCor2	Zheng et al., 2017	https://emcore.ucsf.edu/ucsf-motioncor2
CtfFind-4.1	Rohou and Grigorieff, 2015	https://grigoriefflab.umassmed.edu/ctffind4
Relion 3.1	Scheres, 2016	https://www3.mrc-lmb.cam.ac.uk/relion/index.php?title=Main_Page
cryoSPARC	Punjani et al., 2020	https://cryosparc.com/
UCSF Chimera	Petterson et al., 2004	https://www.cgl.ucsf.edu/chimera/
UCSF Chimera X	Petterson et al., 2021	https://www.cgl.ucsf.edu/chimerax/
SWISS-MODEL	Waterhouse et al., 2018	https://swissmodel.expasy.org/
COOT v0.9.2 EL	Emsley et al., 2010	https://www2.mrc-lmb.cam.ac.uk/personal/pemsley/coot/
Phenix v1.17.1–3660	Liebschner et al., 2019	https://www.phenix-online.org/
PyMol Molecular Graphics System	Schrodinger	https://pymol.org/2/
VMD v1.9.3	Humphrey et al., 1996	https://www.ks.uiuc.edu/Research/vmd/
Epock v1.0.5	Laurent et al., 2015	https://epock.bitbucket.io/
Other		
UltrAuFoil gold grids	Quantifoil	Au300-R1.2/1.3
Superdex 75 10/300 GL gel filtration column	Cytiva	Cat#17517401
Superdex 200 10/300 GL gel filtration column	Cytiva	Cat#17517501
MonoQ 10/100 GL anion exchange column	Cytiva	Cat#17516701
Glutathione Sepharose 4B resin	Cytiva	Cat#17075604